Second-order hydrodynamic effects on the response of three semisubmersible floating offshore wind turbines

Zhang, L., Shi, W., Karimirad, M., Michailides, C., & Jiang, Z. (2020). Second-order hydrodynamic effects on the response of three semisubmersible floating offshore wind turbines. *Ocean Engineering*, *207*, Article 107371. https://doi.org/10.1016/j.oceaneng.2020.107371

Published in:
Ocean Engineering

Document Version:
Peer reviewed version

Second-order hydrodynamic effects on the response of three semisubmersible floating offshore wind turbines

Lixian Zhang [1], Wei Shi [1, 2, *], Madjid Karimirad [3], Constantine Michailides [4] and Zhiyu Jiang [5]

[1]DeepWater Engineering Research Centre, Dalian University of Technology, China;
[2]State Key Laboratory of Hydraulic Engineering Simulation and Safety, Tianjin University, China;
[3]Civil Engineering, School of Natural and Built Environment, Queen's University Belfast, UK;
[4] Civil Engineering and Geomatics, Cyprus University of Technology, Cyprus;
[5] Department of Engineering Sciences, University of Agder, Grimstad, Norway;

* Corresponding author: Dr. Wei Shi, Email: weishi@dlut.edu.cn

Abstract: Floating structures have become the most feasible solution for supporting wind turbines when offshore wind project move to deeper water. In this paper, a hydrodynamic analysis of three different semisubmersible floating offshore wind turbines is carried out including second-order hydrodynamic effects. The three examined platforms are V-shaped semisubmersible, Braceless semisubmersible and OC4-DeepCwind semisubmersible and are used to support the NREL 5 MW reference wind turbine. The main objective of the present study is to investigate and compare the hydrodynamic response of the three different semisubmersible floaters in two water depths (100 m, and 200 m) under different load conditions. The effects of second-order wave loads on the platform motions and mooring tension are discussed and compared by using different methods including Newman's approximation and the full QTF (Quadratic transfer function) method. The drag effect on the structure motion response is also discussed in this paper. The comparison presented is based on statistical values and response spectra of floating platform motions as well as mooring tensions. The results show that the dynamic response of semisubmersible FOWTs (floating offshore wind turbines) is overestimated when ignoring the Morison drag effect on the columns of the semisubmersible FOWT. The second-order difference wave loads can excite the resonance of motion especially for the platform-pitch motion, which could cause structural failures. The full QTF method should be used to calculate the second-order wave force to better simulate the realistic dynamic response of semisubmersible FOWTs.

Keywords: Hydrodynamic loads; Second-order wave loads; Semisubmersible floating wind turbines; Newman's approximation; Quadratic transfer function.

1. Introduction

Wind energy has experienced rapid development in recent years, moving from onshore to offshore. At the end of 2018, 18,499 MW of installed wind turbine power capacity from a total of 4,543 offshore wind turbines was installed (DeCastro *et al.*, 2019). Most offshore wind turbines are installed in shallow water with bottom-fixed foundations (Shi *et al*., 2015, 2016; Mo *et al*, 2017; Chian *et al*, 2018). In many countries, including China, Norway and the USA, the main portion of offshore wind resources is found in deep water, where the bottom-fixed supporting structures are not economically feasible. Floating offshore wind turbines (FOWTs) provide a promising solution in deep water areas. In China, the offshore resources in shallow water are estimated to be 750 GW at 10 m height, while the offshore resources in deep water are estimated to be 1740 GW (Hong and Möller, 2011). To explore the wind energy in deep water sites, many concepts have been proposed for FOWTs, by utilizing technology and experience from the offshore oil and gas industry. Based on the principles adopted to achieve static stability, floating support platforms can be classified into three primary concepts: semisubmersible, spar buoy and Tension Leg Platform (TLP). Some designs are in the prototype stage including the full-scale projects Hywind demo (Driscoll *et al*., 2016) in Norway, WindFloat (Maciel, 2010) in Portugal, Fukushima phase II FOWT (Boccard, 2014) in Japan and Hywind Scotland (Skaare, 2017) in the UK etc. Compared to spar buoy and TLP, the semisubmersible platform is more feasible in various water depths and has low installation costs of the mooring system. The semisubmersible platform has better hydrodynamic behaviour due to the deep draft. Several concepts of semisubmersible floating offshore wind turbines have been proposed including WindFloat (Roddier et al., 2010), Dutch Tri-floater (Huijs et al., 2014), Windsea (Lefranc et al., 2011), Windflo (Le Boulluec et al., 2013), Braceless (Luan et al., 2016), V-shaped (Karimirad and Michailides, 2015), OC4-DeepCwind (Robertson et al., 2014) semisubmersible FOWTs.

Currently, several numerical simulations of FOWTs(Antonutti *et al*., 2016; Jiang *et al*., 2018; Shi *et al*., 2019; Zhao *et al*., 2019) have been carried out to investigaite the dynamic performance of semisubmersible FOWTs using first-order radiation and diffraction. However, the offshore oil and gas industry has demonstrated the importance of second-order hydrodynamic load for certain floating platform. The second-order wave loads mainly include mean drift force, sum- and difference-frequency wave loads. The sum-frequency and difference-frequency loads can excite offshore structures' eigenfrequencies, and may result in large oscillations that cause damage to the floating structures. Roald et al.(2013) assessed the importance of second-order wave forces on OC3-Hywind spar and the UMaine TLP. The results show that the second-order wave forces are very small for OC3-Hywind, while those are quite high on UMaine TLP. Coulling et al.(2013) used Newman's approximation method in FAST to consider the effect of second-order wave force on OC4-DeepCwind semisubmersible FOWT. The results show that the second-order difference-frequency wave-diffraction forcing played a significant role in the global response of the DeepCwind semi-submersible FOWT. Li et al. (2017) proposed a new concept of FOWT and investigated the hydrodynamic response of the floating platform with an emphasis on the computation of second-order difference-frequency wave loads and their effects on the global rigid-body motion response. Xu et al. (2018) assessed the importance of second-order hydrodynamics on the Braceless semisubmersible floating offshore wind turbine concept using Newman's approximation and the full QTF method. Gueydon et al. (2014) used different codes including FAST and aNySIM to investigate the second-order effect on OC4-DeepCwind semisubmersible FOWT. The results show that the second-order sum-frequency loads appeared to have negligible effects on the motions while the effects of difference-frequency load were larger. The loads and responses of the system caused by the second-order hydrodynamics were analyzed and compared to the first-order hydrodynamic loads and induced motions in the frequency domain by Bayati et al (2018).

In this paper, the main objective is to investigate hydrodynamic effects on the response of three different semisubmersible floating offshore wind turbines, including the V-shaped semisubmersible FOWT, the Braceless semisubmersible FOWT and the OC4-DeepCwind semisubmersible FOWT, at different water depths addressing second-order hydrodynamic loads. Hydrodynamic models are developed by using the ANSYS/AQWA tool with the panel method (ANSYS Inc., 2017). Particular attention is given to second-order hydrodynamics loadings using Newman's approximation and the full QTF method. The second-order hydrodynamic loads and resulted responses are analyzed and compared with relevant loads, responses and induced motions in the frequency-domain for different water depths. The effect of the second-order hydrodynamic loads and water depth is examined for all three semisubmersible platforms.

In moderate water depths (40 m to 100 m), dynamic responses of semisubmersible FOWT become larger than those in deep water. For the responses of the three semisubmersible FOWTs at different water depth, the results show that the Braceless semisubmersible FOWT is more sensitive in shallow water depth. For the first-order solution, Morison drag term has a significant impact on the platform motion showing that Morison drag term should also be considered for better simulating the actual motion responses. Furthermore, it is found that the heave natural frequency of OC4-DeepCwind semisubmersible FOWT is close to the normal wave frequency range, which could cause large resonance and then cause the failure of the structure. For second-order solution, motion responses can be excited when considering second-order wave loads. The results show that the pitch motion can be greatly excited when using the full QTF method. Compared to the pitch motion responses of three semisubmersible FOWTs at different water depth, the contribution of second-order wave loads to the pitch motion increasing when the water depth decreases. Therefore, the full QTF method should be used in the numerical simulation of semisubmersible FOWTs to better capture the effect of second-order wave loads. The results presented in this paper may help resolve the fundamental design trade-offs between different FOWTs.

2. Theoretical background

It is important to design floating offshore wind turbines considering fluid-structure-interaction. The force on the floating structures and motion of the platform caused by these interactions is one of the main subjects of marine hydrodynamics. The hydrodynamics are mainly divided into two parts: the influence of fluid motions on the structures (diffraction), and the influence of moving structures that lead to the wave generation (radiation). Hydrostatics should also be accounted for to consider the effects of buoyancy and hydrostatic restoring forces. The hydrodynamic loads can be estimated by using the Morison equation, potential flow theory, hybrid methods or higher fidelity numerical modelling techniques (e.g. computational fluid dynamics (CFD)). The Morison Equation is mainly used to calculate the hydrodynamic loads for slender structures with small diameters compared with the wavelength. For large-volume structures, diffraction and radiation are relatively important and potential flow theory is used to calculate the hydrodynamic loads acting on the platform.

2.1 Potential flow theory

The potential flow theory *(*Faltinsen, 1993; Teng, 2015) is used to calculate the hydrodynamics when designing marine structures. Potential flow theory considers the flow around a body to be incompressible, inviscid, and irrotational, with negligible surface-tension effects. The hydrodynamic loads that usually affect the response of floating wind turbines consist of two parts: first-order wave loads and second-order wave loads.

2.1.1 First-order wave loads

For the first-order wave calculations, the load on the structure and platform motion have zero mean value and oscillate with the frequency of the incident wave (Faltinsen, 1993). First-order hydrodynamic wave load including incident wave loads, diffraction wave loads and radiation wave loads can be described by:

$$\vec{F} = \vec{F}_I + \vec{F}_D + \vec{F}_R \tag{1}$$

$$\vec{F}_I + \vec{F}_D = -\int_s i\omega\rho_\mathrm{w}\phi_i\vec{n}_\mathrm{j}\mathrm{d}s - \int_s i\omega\rho_\mathrm{w}\phi_\mathrm{d}\vec{n}_\mathrm{j}\mathrm{d}s \tag{2}$$

$$\vec{F}_R = -\ddot{x}_k \frac{\rho_\mathrm{w}}{\omega}\int_s \phi_{\mathrm{ik}}^{\mathrm{Re}}\vec{n}_\mathrm{j}\mathrm{d}s - \dot{x}_k\rho_\mathrm{w}\int_s \phi_{ik}^{\mathrm{Im}}\vec{n}_\mathrm{j}\mathrm{d}s = -A_{\mathrm{jk}}\ddot{x}_k - B_{\mathrm{jk}}\dot{x}_k \tag{3}$$

where $\vec{F}_I$ is the incident wave load; $\vec{F}_D$ is the diffraction wave load; $\vec{F}_\mathrm{R}$ is the radiation wave load; ω is the circular frequency of the wave; $\vec{n}$ is the normal direction vector of the wet surface; s is the area of the wet surface immersed in water; ϕ_i is the incident potential of the wave without the perturbation of the body; ϕ_d is the diffraction potential of the wave when the waves pass through the body; ρ_w is the density of the water; $\vec{n}_\mathrm{j}$ is a direction vector; ϕ_{ik}^{Re} and ϕ_{ik}^{Im} are the real and imaginary parts of the incident potential of the wave without the perturbation of the body, respectively; A_{jk} and B_{jk} are the added mass and radiation damping coefficients. The indices k and j refer to the degrees of freedom (DOFs) of the platform.

2.1.2 Second-order wave loads

Second-order hydrodynamic loads are proportional to the square of the wave amplitude and have frequencies that are equal to both the sum and the difference of pairs of incident wave frequencies. This means that, although the natural frequencies of the structure are designed to be outside the first-order wave energy spectrum, the second-order loads may excite these frequencies. Therefore, despite the normally small second-order hydrodynamic loads, the resonant effect may be significant. Second-order wave exciting forces can be described in the frequency domain by decomposition into three terms (Newman, 1967; Fonseca *et al*.,2008; Pessoa *et al*., 2010):

(1) Mean drift force $\overline{F}_{mean}^2$, which is a frequency-dependent mean value;

(2) Difference-frequency wave drift force $\overline{F}_{diff}^2$, which oscillates at difference-wave frequencies;

(3) Sum-frequency wave force $\bar{F}^2_{sum}$, which oscillates at sum-wave frequencies.

According to Pinkster (Pinkster, 1975), the second-order wave forces can be written as the summation of five different components when they are determined by direct pressure integration.

$$
\begin{aligned}
\bar{F}^2 = & -\oint_{WL} \frac{1}{2}\rho g \xi_r^{(1)} \cdot \xi_r^{(1)} \vec{n}\, dl && \text{I} \\
& + \iint_{S_0} \frac{1}{2}\rho \left|\nabla \phi^{(1)}\right|^2 \vec{n}\, ds && \text{II} \\
& + \iint_{S_0} \rho \left(X \cdot \nabla \frac{\partial \phi^{(1)}}{\partial t} \right) \vec{n}\, ds && \text{III} \\
& + M_s R \cdot \ddot{X}_g && \text{IV} \\
& + \iint_{S_0} \rho \frac{\partial \phi^{(2)}}{\partial t} \vec{n}\, ds && \text{V}
\end{aligned}
\qquad (4)
$$

where ρ is the density of the water; g is the gravitational acceleration; $\vec{n}$ is The direction of the normal; $\phi^{(1)}$ is the first-order velocity potential; WL is the waterline; $\xi_r^{(1)}$ is the relative wave elevation; S_0 is the mean wetted surface of the floating body; X is the motion of the floating body; M_s is mass of the floating body; M_s is the mass matrix of floating structure; R is the rotational transformation matrix of floating structure; $\ddot{X}_g$ is the acceleration of the center of gravity; $\phi^{(2)}$ is the second-order velocity potential.

Components I to IV represent the mean drift force which is determined from the first-order solution. The mean drift force can be calculated by using the far-field method or near-field method. The accuracy of the far-field method is higher than that of the near-field method, but it can calculate the force in only three DOFs. By contrast, near-field solution can be used to calculate second-order wave forces on a floating body in 6 DOFs. Therefore, the near-field method is employed in the present paper to calculate the mean drift force based on the mean wetted body surface integration approach.

With regards to the semisubmersible floating offshore platform, the slow drift wave force (term 5) including the difference-frequency force becomes more significant. The difference-frequency is close to the natural frequency of the semisubmersible platform which could cause the resonance of the floating system and could damage the structure. The fifth component of equation (4) involves the second-order velocity potential that can be calculated directly by using the near-field solution (the full QTF method). Compared to Newman's approximation method, the complete QTF matrix gives more accurate estimations of the low-frequency loads; However, it requires the solution to the second-order problem and the time series reconstruction is more time-demanding. Therefore, Newman's approximation method is proposed, mainly to avoid computing the second-order velocity potential $\phi^{(2)}$ and to improve computational efficiency. For Newman's approximation, the drift force can be described by:

$$P_{ij}^{-} = 0.5 a_i a_j \left(\frac{P_{ii}^{-}}{a_i^2} + \frac{P_{jj}^{-}}{a_j^2} \right) \tag{5}$$

$$Q_{ij}^{-} = 0 \tag{6}$$

where P_{ii}^{-} , P_{jj}^{-} , Q_{ii}^{-} and Q_{jj}^{-} are calculated from second-order mean drift force solution. Therefore, quadratic transfer functions (QTF) including P_{ij}^{-} , Q_{ij}^{-} can be calculated.

For semisubmersible floating platforms, the most significant part of the dynamic response is at both the wave frequency and the structure natural frequency region. Therefore, only the mean drift force and slowly varying drift force will be discussed since the difference-frequency value is close to the natural frequency of the semisubmersible floating platform.

2.2 Viscous load

In the potential flow theory, the viscous effect from the flow is ignored. In order to take into account the viscous force, the drag term of the Morison equation is used. The viscous drag term of the Morison equation for the fluid force acting on the cross-section of a slender structural member is

$$dF_{vicous} = 0.5 \rho C_d A \left| u_f - u_s \right| \left(u_f - u_s \right) dl \tag{7}$$

where C_d is the drag coefficient; A is the projected area of a unit length cylinder perpendicular to the flow direction ; u_f is the fluid particle velocity; u_s is the structure's velocity.

2.3 Mooring system

In this paper, the lumped mass method (Hall and Goupee,2015) is adopted to discretize the cable dynamics over the length of the mooring line. In this approach, as seen in Figure 1, the mooring line is discretized into N evenly-sized line segments connecting N+1 node points. The right-handed inertial reference frame is defined with the Z-axis being measured positive up from the water plane. The location of each node point i is defined by the vector P_i which contains the node position in x, y and z-direction. Each segment S_i of a cable element has identical properties of unstreched length l, diameter d ,density ρ ,Young's modulus E , and damping coeifficent C_{int} . And the cable model combines internal axial stiffness and damping forces with weight and buoyancy forces, hydrodynamic forces from Morison equation, and forces from contact with the seabed.

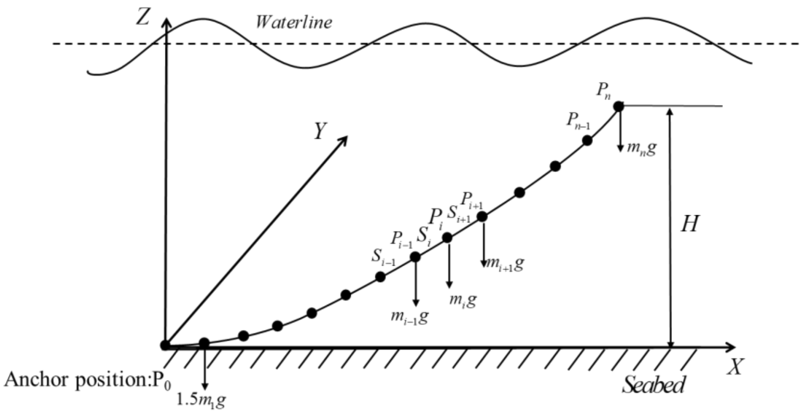

Figure 1. Mooring line discretization

2.4 Equation of motion

The semisubmersible floating structure is represented by a six degree of freedom (6-DOF) rigid body. The load model for the body accounts for the wave loads;It is stated that in the present paper, the emphasis is on the study of the hydrodynamic loads. The equation of motion under wave loads in time domain is calculated in ANSYS/AQWA; for the rigid body motions, j, and it can be expressed as:

$$\sum_{i=1}^{6}\left(\left(M_{ij}+A_{ij}\right)\ddot{x}_j(t)+\int_{-\infty}^{t}\dot{x}_j(\tau)K_{ij}\left(t-\tau\right)d\tau+C_{ij}x\left(t\right)\right)=F_{wave,j}\left(t\right)+F_{moor,j}\left(t\right) \tag{8}$$

where M_{ij} is the mass coefficient, A_{ij} is the added mass coefficient calculated by AWQA-LINE, $K_{ij}\left(t-\tau\right)$ is the retardation function which represents the fluid memory effect, C_{ij} is the restoring coefficient calculated by AWQA-LINE, $\ddot{x}$, $\dot{x}$ and x are the acceleration, velocity, and displacement of the platform, $F_{wave,j}\left(t\right)$ is the wave exciting force, $F_{moor,j}\left(t\right)$ is the restoring force that results from mooring lines, *j* is the DOF in surge, sway, heave, roll, pitch and yaw direction.

3. Numerical model of the semisubmersible FOWTs

3.1 Wind turbine model

Different from the traditional marine floating structures, the large height of the wind turbine could cause instability of the floater. Although the wind effect is not included in the present paper which means the wind turbine is in a parked condition, the weight of wind turbines components is considered during the simulation. The wind turbine used in this paper was developed by the National Renewable Energy Laboratory (NREL), USA. It is a conventional three-bladed, upwind, variable-speed, collective-pitch controlled horizontal axis wind turbine. The geometric properties of the wind turbine and tower are listed in Table 1 (Jonkman *et al*., 2009).

Table 1. Main properties of NREL-5 MW baseline wind turbine and tower (Jonkman *et al*., 2009).

Parameter	Value
Rated power	5 MW
Nacelle mass kg	240,000
Rotor mass kg	110,000
Wind turbine (WT) Center of Gravity(CoG) m	(-0.2,0.0,70)
Total mass of WT kg	600,000
Total WT mass moment of inertia about X axis(Ixx) kg*m^2	3,770,000,000
Total WT mass moment of inertia about Y axis(Iyy) kg*m^2	3,660,000,000
Total WT mass moment of inertia about Z axis(Izz) kg*m^2	112,000,000
Elevation to tower base above MSL m	10
Center of Gravity(CoG) location of tower above MSL m	43.4
Overall tower mass kg	250.,000

3. 2 Semisubmersible floating platform model

Three different semisubmersible floating platforms, including (1) the V-shaped semisubmersible floating platform, (2) the Braceless semisubmersible floating platform and (3) the OC4-DeepCwind semisubmersible floating platform, were considered to support the NREL 5 MW wind turbine at two different water depths. The water depth is assumed to be 100 m and 200 m for each concept. The three floating structures are illustrated in Figure 2 and their properties are summarized in Table 2.

Table 2. Properties for the three semisubmersible platforms.

Parameter	**V-shaped Semi**	**Braceless Semi**	**OC4-DeepCWind Semi**
Water depth m	200/100	200/100	200/100
Freeboard m	20	20	12
Draft m	28	30	20
Submerged volume m^3	10,013	10,517	13,917
Floater steel mass kg	1,630,000	1,686,000	3,852,000
Total mass (Including WT) kg	10,300,000	10,780,000	14,070,000
COG (x, y, z) m, m, m	(-30.6,0, -16)	(0,0, -18.9)	(0,0, -9.89)
I_{xx} w.r.t. COG kg*m^2	12,900,000,000	10,650,000,000	10,110,000,000
I_{yy} w.r.t. COG kg*m^2	21,800,000,000	10,650,000,000	10,110,000,000
I_{zz} w.r.t. COG kg*m^2	17,900,000,000	8,412,000,000	12,779,000,000

(a) (b) (c)

Figure 2. Semisubmersible FOWT systems. (a) V-shaped Semi; (b) Braceless Semi; (c) OC4-DeepCwind Semi.

The V-shaped semisubmersible FOWT is designed by Karimirad and Michailides (2015) according to the concept of semisubmersible FOWT in project Fukushima FORWARD (Forward, 2014). It consists of one main column and two side columns connected by two pontoons. Different from the other two semisubmersible platforms, V-shaped semisubmersible FOWT is not a symmetrical floating platform, which the NREL 5 MW wind turbine is at the top of the main column. It must be noted that V-shaped semi FOWT maintains the balance by setting different ballast heights for each column. More detailed properties of the V-shaped semisubmersible FOWT are summarized in (Karimirad and Michailides, 2015; Karimirad and Michailides, 2016).

The Braceless semisubmersible FOWT is designed by Luan et al. (2016) in Norwegian University of science and technology (NTNU) according to the concept of OO-Star semisubmersible FOWT(Borisade, 2016). It is mainly composed of three side columns and one central column. It is noted that the Braceless semisubmersible FOWT is symmetrical with NREL 5 MW wind turbine on the centre column. Three pontoons are used to connect central column and side columns. More detailed information of Braceless semisubmersible FOWT can be found in (Luan, 2018).

The OC4-DeepCwind semisubmersible FOWT is designed by NREL. The OC4-DeepCwind semisubmer sible FOWT consists of one central column and three side columns. It has heave plates at the bottom of the upper columns to reduce the heave motion of the floating system. Several braces including horizontal and diagonal braces are used to connect the columns. Detailed properties of the OC4-DeepCwind semisubmersible FOWT are available in (Robertson *et al*., 2014).

The main reason we chose the aforementioned three semisubmersible FOWTs is that the three semisubmersible FOWT represents different design ideas for semisubmersible FOWTs. The V-shaped semisubmersible FOWT is an asymmetric structure without the bracings. And both Braceless semisubmersible FOWT and OC4-DeepCwind semisubmersible FOWT is symmetric structures with center column supporting the wind turbine systems. Different from OC4-DeepCwind semisubmersible FOWT, Barceless semisubmersible FOWT has no bracings to connect the center column and side columns. Those three semisubmersible FOWTs are different in preliminary design.

3.3 Mooring systems designs for 200 m and 100 m

For the V-shaped semisubmersible FOWT, the mooring system consists of three catenary mooring lines that are made of wire rope. The mooring line is positioned with 150 degrees between the main mooring line (ML 1) and the side mooring lines (ML 2, ML 3), while the angle between ML 2 and ML 3 is 60 degrees. The clump mass of the V-shaped semisubmersible FOWT is positioned at 82 m far from the fairlead of each mooring line for both 100 m and 200 m. The relevant characteristics of the mooring line are shown in Table 3 and 4.

The mooring system of Braceless semisubmersible FOWT consists of three catenary mooring lines that are positioned with 120 degrees between the mooring lines. Each mooring line is attached at the outer columns of the semisubmersible FOWT at a water depth of 18 m. The clump masses of the Braceless semisubmersible for 100-m water depth are heavier than those for 200-m water depth, which is designed to maintain the similar pretension and stiffness in different water depths.

The initial OC4-DeepCwind semisubmersible FOWT is designed for 200-m water depth, which has been utilized as a reference model for the mooring system design of 100-m water depth. Based on the original 200-m water depth design, a 100-m water depth mooring line is designed to achieve the similar stiffness (Jeon, *et al*, 2013), pretension and natural frequency of the floating system in surge motion. The properties of the 100-m depth mooring line are kept the same as those of the 200-m water depth mooring lines. A clump mass is also added at each line to achieve similar pretension and stiffness. Detailed mooring line properties and other characteristics of the mooring system are shown in Table 3 and 4.

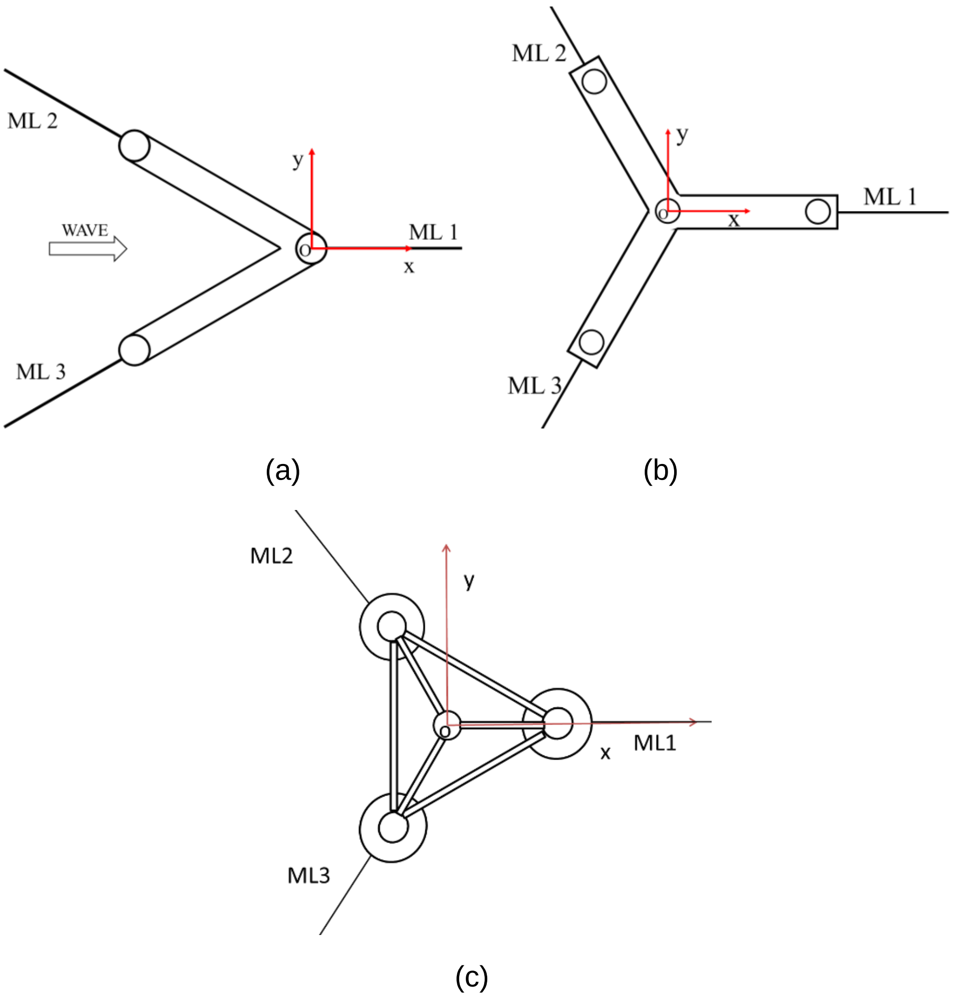

Figure 3. Mooring system configuration of the three platforms. (a) V-shaped Semi; (b) Braceless Semi; (c) OC4-DeepCwind Semi.

Table 3. Properties of the mooring line system at 200-m water depth.

Parameter	V-shaped Semi	Braceless Semi	OC4-DeepCWind Semi
Mooring line length m	700.0	1084.5	835.5
Mooring line type	Spiral rope	Spiral rope	Spiral rope
Number of mooring lines	3	3	3
Equivalent Axial stiffness N	3E9	3.08E9	7.536E8
Mass per unit length kg/m	117	115	108.63
Pretension kN	1680.0	1300.0	1040.0
Diameter of mooring line m	0.138	0.1365	0.0766
Fairlead for ML1 (x, y, z) m	(4.5, 0, -18)	(43, 0, -18)	(40.9,0, -14)
Fairlead for ML2 (x, y, z) m	(-55.8, -32.3, -18)	(-22.1, 38.3, -18)	(-20.4, -35.4, -14)
Fairlead for ML3 (x, y, z) m	(-55.8, 32.3, -18)	(-22.1, -38.3, -18)	(-20.4, 35.4, -14)
Anchor point of ML1 (x, y, z) m	(650, 0, -200)	(1084.4, 0, -200)	-(837.6, 0, -200)
Anchor point of ML2 (x, y, z) m	(-618.7, 357, -200)	(-542.2, 939.1, -200)	(-418.8, 725.4, -200)
Anchor point of ML3 (x, y, z) m	(-618.7,-357, -200)	(-542.2, -939.1, -200)	(-418.8, -725.4, -200)
Clump mass volume m^3	4.4	-	-
Clump mass weight kg	37,000	15,000	-

Table 4. Properties of the mooring line system at 100-m water depth.

Parameter	V-shaped Semi	Braceless Semi	OC4-DeepCwind Semi
Mooring line length m	453.0	891.6	514.0
Mooring line type	Spiral rope	Spiral rope	Spiral rope
Number of mooring lines	3	3	3
Equivalent Axial stiffness N	3E9	3.08E9	7.536E8
Number of mooring lines	3	3	3
Mass per unit length kg/m	117.00	115.00	108.63
Pretension kN	1500.0	1190.0	952.0
Diameter of mooring line m	0.138	0.1365	0.0766
Fairlead for ML1 (x, y, z) m	(4.5, 0, -18)	(43, 0, -18)	(40.9,0, -14)
Fairlead for ML2 (x, y, z) m	(-55.8, -32.3, -18)	(-22.1, 38.3, -18)	(-20.4, -35.4, -14)
Fairlead for ML3 (x, y, z) m	(-55.8, 32.3, -18)	(-22.1, -38.3, -18)	(-20.4, 35.4, -14)
Anchor point of ML1 (x, y, z) m	(434, 0, -100)	(917.0, 0, -100)	(535.0, 0, -100)
Anchor point of ML2 (x, y, z) m	(-433.7, 247, -100)	(-458.5, 794.1, -100)	(-267.5, 463.3, -100)
Anchor point of ML3 (x, y, z) m	(-433.7,-247, -100)	(-458.5, -794.1, -100)	(-267.5, -463.3, -100)
Clump mass volume/m^3	4.4	-	-
Clump mass weight/kg	37,000	15,000	45,000

3.4 Design load cases

Based on the data (Li., *et al*, 2015), Norway site 5 (Figure 4) was selected as a representative site for the simulation. It should be noted that wind loads are not considered in the present paper. The main objective of this paper is to investigate the hydrodynamic characteristics of different semisubmersible FOWT at different water depths with emphasis on the second-order wave loads. Therefore, only wave conditions are considered in the present paper. Three different wave conditions including moderate and extreme conditions are listed in Table 5.

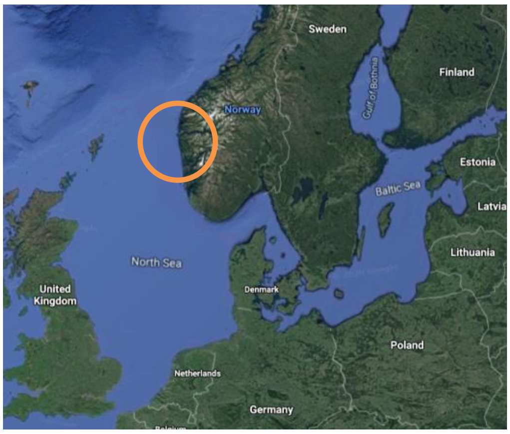

Figure 4. Location of Norway site 5.

Table 5. Load cases for Norway site 5 (Li., *et al*, 2015).

Load case	Hs (m)	Tp (s)
LC 1	3.0	10.0
LC 2	5.0	12.0
LC 3	14.1	13.3

3.5 Numerical setting in the simulation

The hydrodynamic loads are calculated using the boundary element method (BEM) based on potential flow theory and the Morison equation. Potential flow theory is applied on both the columns and pontoons; and, the drag term of the Morison equation is applied to the columns. For the OC4-DeepCwind semisubmersible FOWT, the bracings are modelled using the Morison equation.

In this paper, first-order wave load analysis of the motion in sea states is performed with AQWA-NAUT (ANSYS Inc., 2017), which involves meshing the total wet surface of a structure to create a hydrodynamic and hydrostatic model. The nonlinear Froude-Krylov and hydrostatic wave forces on the instantaneous wetted surface (i.e., beneath the incident wave surface) can be calculated in NAUT. This calculation is performed at each time step, along with the instantaneous values of all other forces. Accurate dynamic or kinematic properties of fluid particles beneath the wave surface are thus required for this purpose. These forces are then applied, via a mathematical model, see Equation (10). The position and velocity at the subsequent time step are found by integrating these accelerations in the time-domain, using a two-stage predictor-corrector numerical integration scheme.

For the second-order hydrodynamic model, the mean drift force can be calculated by using the far-field method or near-field method in the AQWA-DRIF module (ANSYS Inc, 2017). In AQWA-DRIF module, the QTF can be calculated by using the direct-pressure integration method (Pinkster, 1975). Newman's approximation is also used to calculate the second-order wave force.

3.5.1 Panel model

The panel model was developed in ANSYS software and the mapped mesh method is employed to obtain a finer frequency domain simulation result for the semisubmersible FOWTs in the AQWA-LINE module. The number of meshes used for the V-shaped semisubmersible, the Braceless semisubmersible and OC4-DeepCwind semisubmersible models are 11691, 23562 and 14735, respectively. The panel model of the three semisubmersible numerical models is shown in Figure 5.

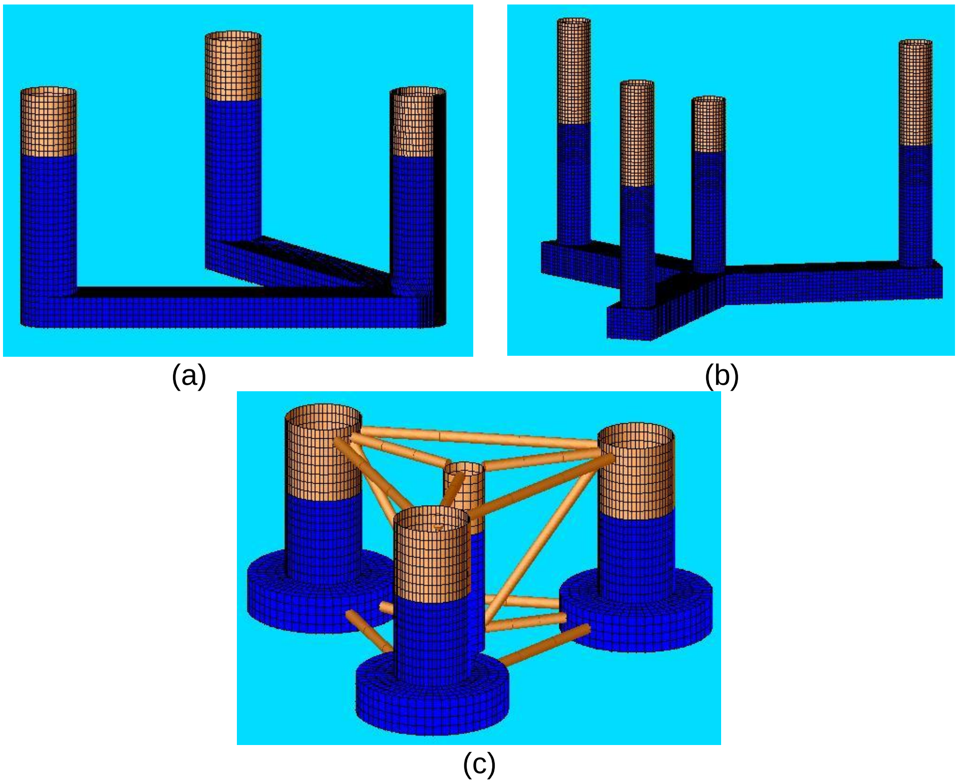

Figure 5. Panel model of the three platforms. (a) V-shaped Semi; (b) Braceless Semi model; (c) OC4-DeepCwind Semi.

3.5.2 Viscous drag model

To calculate the viscous drag of each column and pontoon on the semisubmersible FOWT by the Morison equation, a beam model was used in ANSYS software. Cd depends upon the

Reynolds number, KC number, surface roughness and so on. According to Germanischer Lloyd standard (Wind, 2005), the Cd can be set to 0.70 when the Reynolds number is beyond 2.50E5. In the present simulation, the drag coefficient is set to 0.68 to simulate the viscous drag term on the columns and pontoons.It should be noted that the viscous force on the columns is applied along the transverse direction. Also, the axial viscous drag force is not considered in the present paper. The diameter of columns for the V-shaped semisubmersible (Figure 4(a)) and the Braceless semisubmersible (Figure 4(b)) FOWTs are 9.0 m and 6.5 m respectively. For the OC4-DeepCwind semisubmersible FOWT (Figure 4(c)), the diameters of the bracings, central column, upper column and base column is 1.6 m, 6.5 m, 12.0 m and 24.0 m respectively. For the V-shaped semisubmersible FOWT and Braceless semisubmersible FOWT, the equivalent diameter of pontoons is 7.6 m and 8.3 m, respectively.The diameter of the columns and pontoons was set to 0.01 m to ignore the inertia force from the Morision equation. Futhermore, the drag coefficient is scaled to take into account the modified geometry of the beam model and maintain the same viscous effect contribution as in the real physical model. This is achieved by satisfying the following relation:

$$C_d D = C'_d D' \tag{11}$$

where C'_d and D' are the equivalent drag coefficient and the diameter of the column in the beam model, respectively. The values used in the computation are shown in Table 6.

Table 6. Equivalent drag coefficients and diameters for the Morison model.

Parameters	V-shaped Semi		Braceless Semi		OC4-DeepCwind Semi			
	Column	Pontoon	Column	Pontoon	Braces	Center column	Upper column	Base coulmn
C_a	-	-	-	-	1.0	-	-	-
C_d	0.68	0.68	0.68	0.68	0.68	0.68	0.68	0.68
C'_d	612.0	514.7	442.0	563.7	0.68	442.0	816.0	1632.0
D	9.0	7.6	6.5	8.3	1.6	6.5	12.0	24.0
D'	0.01	0.01	0.01	0.02	1.6	0.01	0.01	0.01

4. Result and discussion

4.1 Response amplitude operator (RAO)

Response amplitude operators (RAOs) can be computed based on the linear wave theory in AQWA. The RAOs show considerable excitation only in the surge, heave, and pitch modes, therefore only these RAOs are presented in Figure 6. The excitation at the other natural frequencies (sway, roll, and yaw) is considerably less because of the zero-degree wave heading.

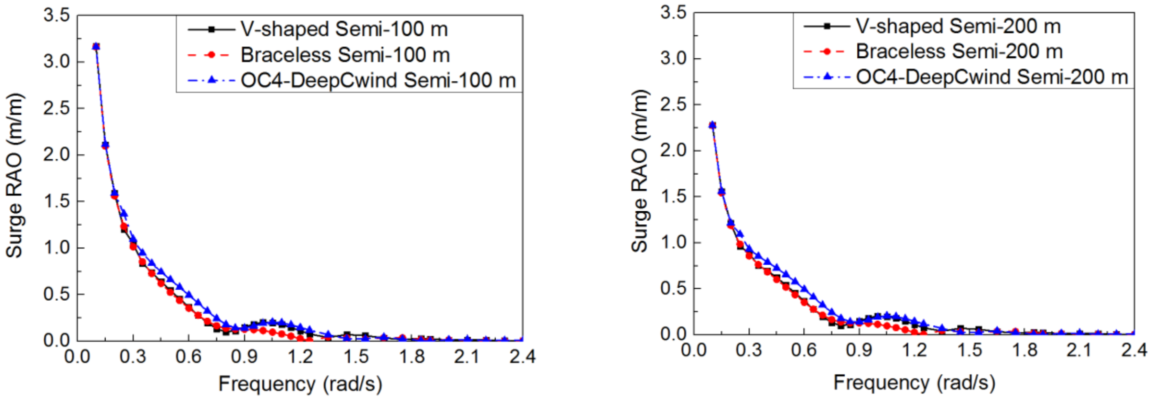

(a)

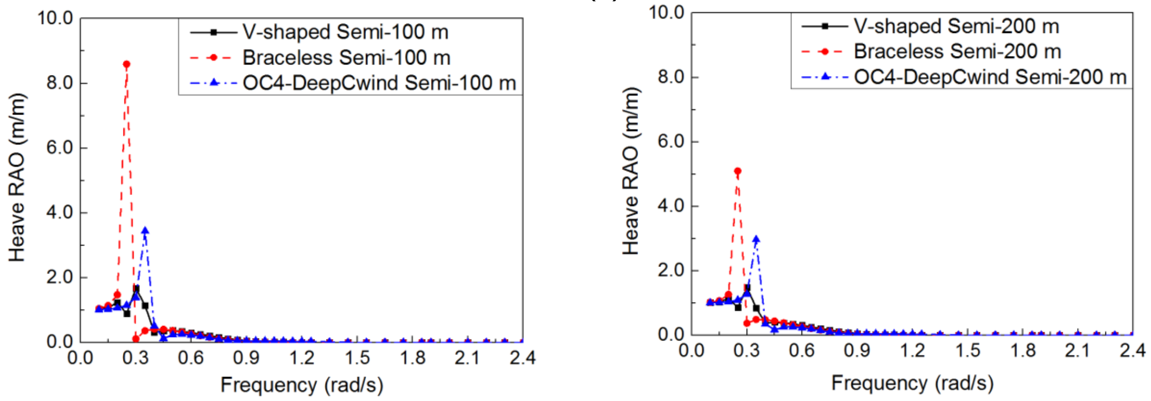

(b)

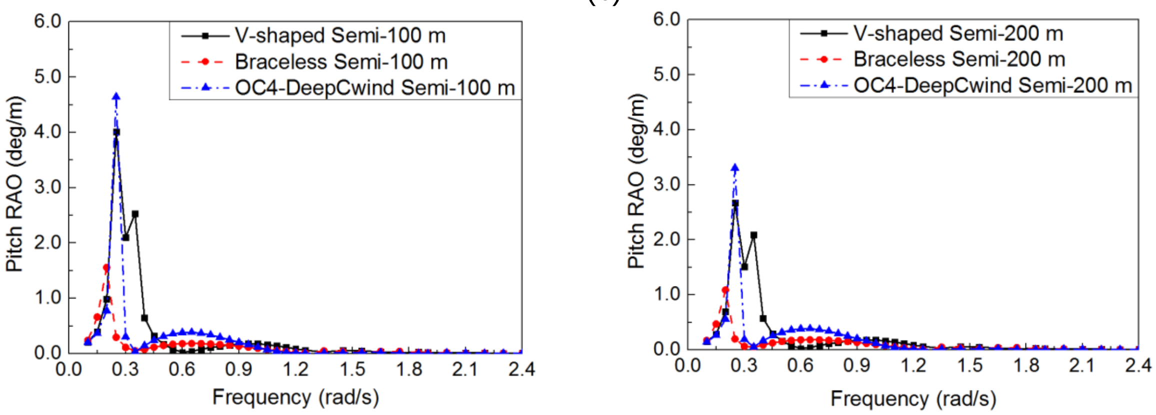

(c)

Figure 6. RAOs of three semisubmersible FOWTs. (a) Surge; (b) Heave; (c) Pitch.

For the surge motion (Figure 6(a)), the results show that the RAOs are similar for the three semisubmersible FOWTs; however, the RAOs are larger at a water depth of 100 m than at a water depth of 200 m. For the heave motion (Figure 6(b)), two peaks are observed for the V-shaped semisubmersible FOWT showing the coupling effect between the heave and pitch motions. A large peak is presented for the heave response at the heave natural frequency of the Braceless semisubmersible FOWT, which is away from the incident wave frequency region (0.3 rad/s to 0.8 rad/s). One peak is also found at the heave natural frequency of the OC4-DeepCwind semisubmersible FOWT, which is close to the wave frequency region. This could cause a large heave motion response when the wave frequency is near the heave natural frequency of the OC4-DeepCwind semisubmersible FOWT. For the pitch motion (Figure 6(c)), there are two peaks observed in the low-frequency region which are in the heave and pitch natural frequency region, for the V-shaped semisubmersible FOWT, and one peak is found at the pitch natural frequency for both the Braceless and OC4-DeepCwind semisubmersible FOWTs. Notably, the pitch motion response in the wave frequency region of the OC4-DeepCwind semisubmersible FOWT is larger than that of the other two platforms. And it can also be observed that the heave and pitch motion responses for the three semisubmersible FOWTs are higher at moderate water depth.

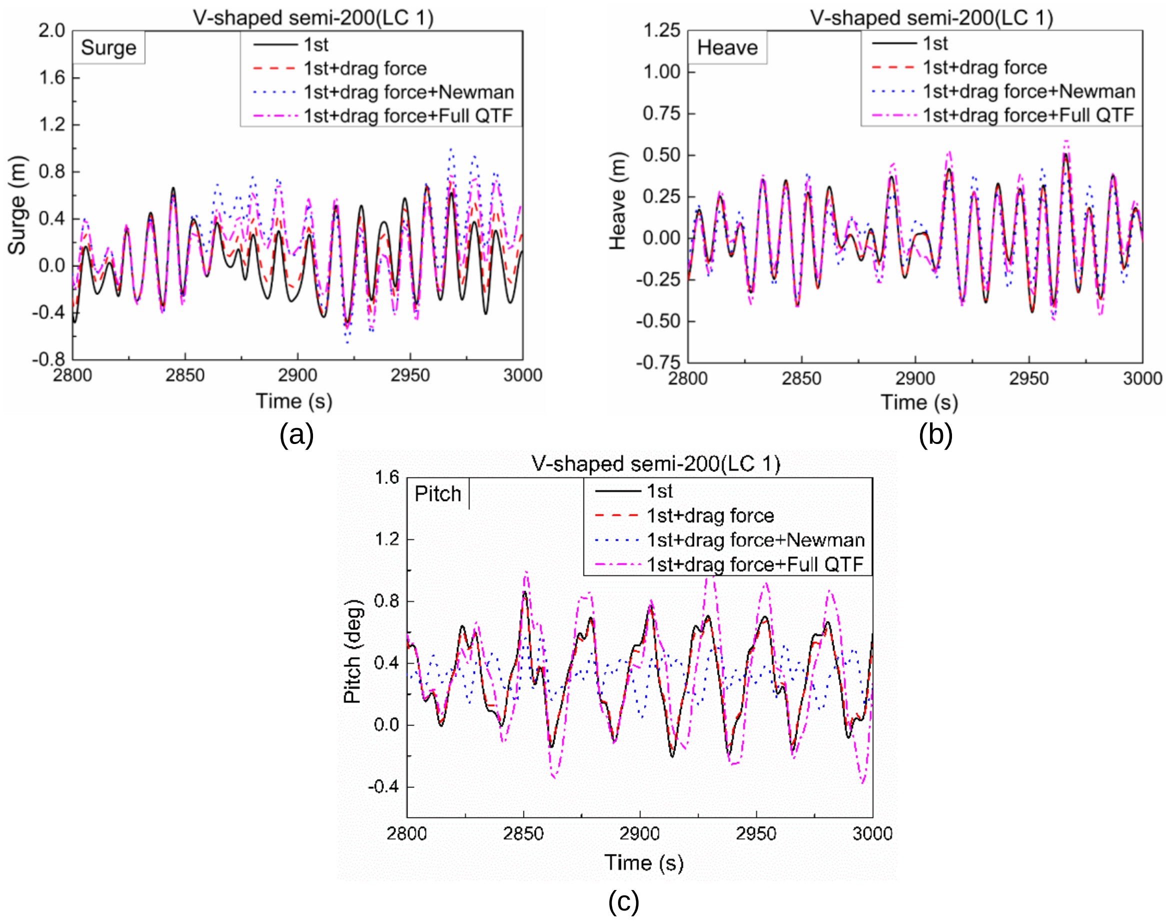

Figure 7. Time-domain motion response of the V-shaped semisubmersible FOWT in LC 1 condition. (a) Surge; (b) Heave; (c) Pitch.

4.1 Time-domain analysis

4.1.1 Motion response

In this section, the time-domain dynamic motion responses of three platforms in different sea conditions with two water depths are estimated. In order to focus on the most critical motion response, only surge, heave and pitch motion are displayed. The total simulation time of the three semisubmersible FOWT is 3500 s, and the first 500 s have not been considered for either for drawing spectrum or statistical results to ignore the transient effect. Due to the limited space in this paper, only the motion time-domain response of the V-shaped semisubmersible FOWT under the LC 1 condition at a 200-m water depth is shown in Figure 7. Moreover, the statistical results of the three semisubmersible FOWTs are discussed in this section.

The effect of the Morison drag term and second-order difference frequency wave force, as well as water depth, were the main focal point. In Figures 8 to 10, the maximum oscillation amplitude of the second-order solution is plotted along with the first-order results.

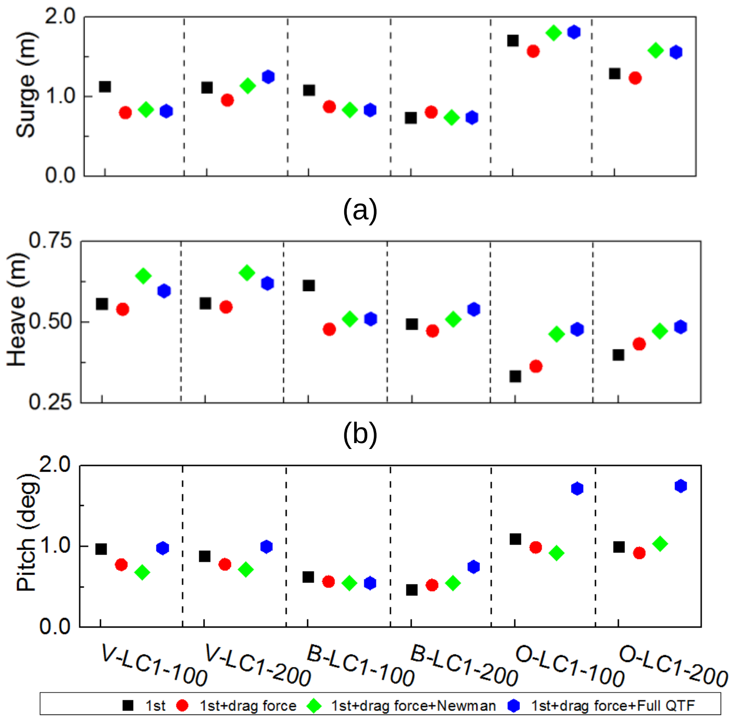

(c)

Figure 8. Maximum values of surge, heave and pitch motion for LC 1 condition. (a) Surge; (b) Heave; (c) Pitch.

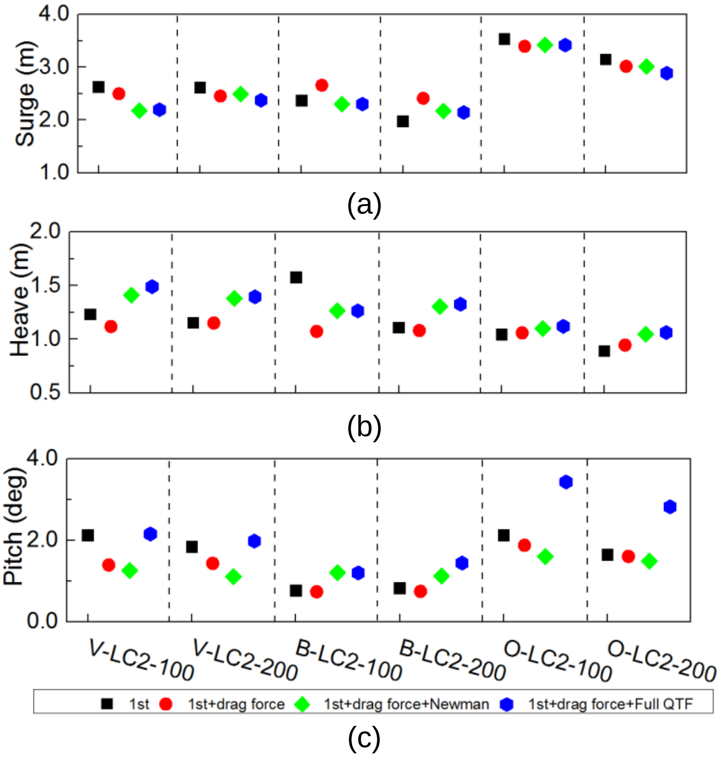

Figure 9. Maximum values of surge, heave and pitch motion for LC 2 condition. (a) Surge; (b) Heave; (c) Pitch.

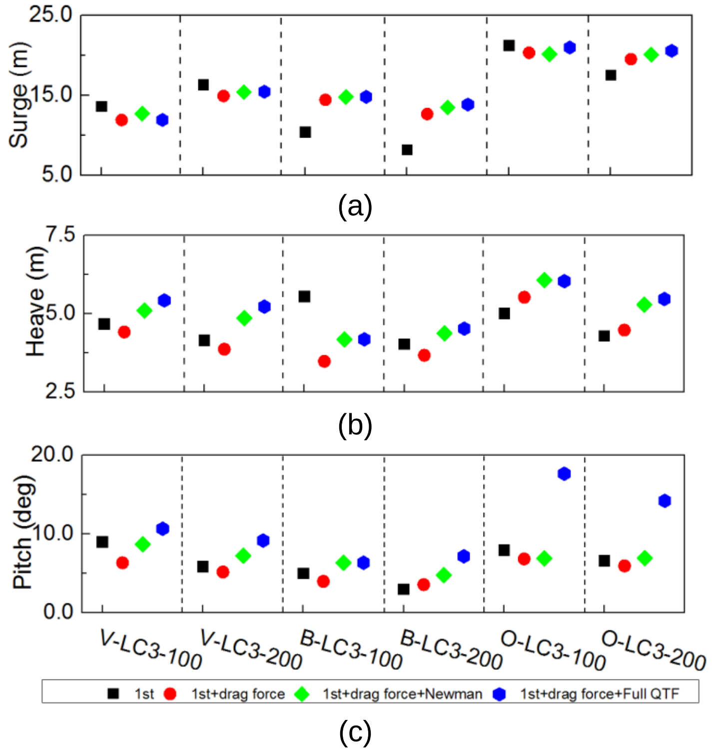

Figure 10. Maximum values of surge, heave and pitch motion for LC 3 condition. (a) Surge; (b) Heave; (c) Pitch.

The following conclusions can be drawn from Figures 8 to Figure 10:

For surge motion, the responses of the OC4-DeepCwind semisubmersible FOWT are larger than those of the other two platforms both at 100-m and 200-m water depths. The results of the first-order solutions show that maximum surge motion responses are larger than those considering the drag term effect for the V-shaped semisubmersible and OC4-DeepCwind semisubmersible FOWTs. For the second-order solution, the maximum surge motion responses are similar for the three semisubmersible FOWTs, showing that Newman's approximation solution considering the second-order effect is enough for the surge DOF.

For heave motion, the maximum motion response of the OC4-DeepCwind semisubmersible FOWT is lower than those of the other two platforms under moderate sea conditions, while it is larger than those of the other two platforms in extreme sea conditions. As shown in Figure 4(b), the RAOs of heave motion for the OC4-DeepCwind semisubmersible FOWT is lower than those for the other two FOWTs when the frequency is greater than 0.5 rad/s. Therefore, under moderate sea conditions where the wave frequency is greater than 0.5 rad/s, the responses of heave motion are lower for the OC4-DeepCwind semisubmersible FOWT than for the other two platforms. However, the wave peak period in the extreme sea state (LC 3) is close to the heave natural period of the OC4-DeepCwind semisubmersible FOWT, which excites the heave motion response of the OC4-DeepCwind semisubmersible FOWT. For the first-order solution, the Morison drag term has limited impact on the heave motion. For the second-order solution, the second-order wave force can greatly excite the heave motion response, while the difference in maximum heave motion responses between the solution from Newman's approximation solution and the full-QTF solution is small.

For the pitch motion, these figures also reveal that the second-order wave force effects are important responses concering the first-order results. As seen in Figure 8(c), Figure 9(c) and Figure 10(c), the pitch responses of second-order solutions are larger than those of first-order solutions, showing that the second-order wave forces should be thoroughly considered especially under extreme sea condition(LC 3). Compared with Newman's approximation method, the full-QTF method is more accurate for the calculation of second-order wave forces. As observed in the plots, the pitch motion responses can be greatly excited when using the full-QTF method, especially for the OC4-DeepCwind semisubmersible FOWT. Under extreme sea condition (LC 3), the amplitude of pitch motion is around 10 degrees, while those are almost 18 degrees for the OC4-DeepCwind semisubmersible FOWT. It also can be observed that the contribution of second-order wave forces to the pitch motion increasing when the water depth decreases. Therefore, full-QTF method is needed for the calculation of second-order wave forces to better capture the actual motion dynamic response for semisubmersible FOWTs.

For the moderate sea conditions, there is a great similarity regarding the standard deviation (STD); therefore, only the STD values from the LC 1 condition and LC 3 condition are listed. Tables 7 and 8 show the standard deviation (STD) results of the three semisubmersible FOWTs under different water depths in the LC 1 and LC 3 condition.

Table 7. STD values of motion response for the three semisubmersible FOWTs under LC 1.

Motion	Method	V-100-LC1	V-200-LC1	B-100-LC1	B-200-LC1	O-100-LC1	O-200-LC1
Surge	1st	***0.32***	***0.30***	***0.32***	***0.22***	***0.47***	***0.45***
	1st+drag force	***0.24***	***0.25***	***0.24***	***0.23***	***0.36***	***0.36***
	1st+drag force+Newman	0.27	0.31	0.26	0.24	0.44	0.44
	1st+drag force+Full QTF	0.27	0.30	0.27	0.25	0.45	0.45
Heave	1st	0.19	0.18	0.21	0.17	0.13	0.13
	1st+drag force	0.19	0.18	0.21	0.17	0.13	0.13
	1st+drag force+Newman	***0.20***	***0.18***	***0.15***	***0.15***	***0.13***	***0.13***
	1st+drag force+Full QTF	***0.20***	***0.19***	***0.23***	***0.19***	***0.13***	***0.13***
Pitch	1st	0.22	0.19	0.19	0.15	0.39	0.35
	1st+drag force	0.21	0.17	0.16	0.14	0.34	0.32
	1st+drag force+Newman	***0.22***	***0.11***	***0.15***	***0.15***	***0.29***	***0.30***
	1st+drag force+Full QTF	***0.30***	***0.26***	***0.21***	***0.19***	***0.56***	***0.61***

Table 8. STD values of motion response for the three semisubmersible FOWTs under LC 3.

Motion	Method	V-100-LC3	V-200-LC3	B-100-LC3	B-200-LC3	O-100-LC3	O-200-LC3
Surge	1st	***3.73***	***3.77***	***3.18***	***2.05***	***6.49***	***4.40***
	1st+drag force	***2.90***	***3.15***	***2.95***	***2.54***	***4.16***	***3.79***
	1st+drag force+Newman	2.76	3.34	3.36	2.92	4.06	4.08
	1st+drag force+Full QTF	2.71	3.24	3.49	3.00	4.08	4.00
Heave	1st	1.56	1.37	1.97	1.44	2.09	1.70
	1st+drag force	1.48	1.38	2.28	1.46	2.06	1.73
	1st+drag force+Newman	***1.54***	***1.41***	***1.34***	***1.31***	***2.19***	***1.83***
	1st+drag force+Full QTF	***1.84***	***1.64***	***2.07***	***1.61***	***2.23***	***1.86***
Pitch	1st	2.73	2.03	1.37	0.88	2.60	2.13
	1st+drag force	2.69	2.19	1.72	1.03	1.96	1.74
	1st+drag force+Newman	***2.56***	***2.06***	***2.25***	***1.54***	***1.88***	***1.63***
	1st+drag force+Full QTF	***4.12***	***3.46***	***2.70***	***2.04***	***5.69***	***4.62***

The surge motion response shows that the STD value of each semisubmersible FOWT is larger when ignoring the Morison drag term. Comparing the results from different second-order solutions, the maximum surge motion is similar for the three semisubmersible FOWTs. These results indicate that together with the maximum values in surge motion, the accuracy of the second-order wave force can be ensured in surge motion by using Newman's approximation method. Notably, the Morison drag force applied to each column is the transverse drag force.

Therefore, it has little impact on the heave motion response as shown in Tables 7 and 8. As it is can be observed in Tables 7 to Table 8, the STD value of the heave motion response increased dramatically for the V-shaped semisubmersible and Braceless semisubmersible FOWTs when using the full QTF method.

For the pitch motion, the STD values of three semisubmersible platforms changes dramatically, especially for the OC4-DeepCwind semisubmersible FOWTs. Tables 7 and 8 also show that the STD value of the motion response is larger at a moderate water depth than those at a water depth of 200 m, showing that the motion response of semisubmersible FOWTs should be thoroughly considered at moderate water depths. It is worth noting that the STD value of pitch motion responses for the three semisubmersible FOWT is much larger in full-QTF solution. Under extreme condition (LC 3), the STD value of pitch motion for these three semisubmersible FOWT at 200 m water depth is increased by 67.0%, 32.0% and 183.4% respectively when using the full-QTF method. As we can see under the extreme sea condition of the full QTF solution, when water depth decreases, the STD of the pitch responses for the V-shaped semisubmersible, Braceless semisubmersible and OC4-DeepCwind semisubmersible FOWT is increased by 19.08%, 32.35% and 23.16% respectively, showing that the Braceless semisubmersible FOWT is more sensitive to the change of water depth.

In general, the platform motion responses are larger when considering the second-order force using the full QTF method. In other words, the maximum and STD values of the motion responses indicate the need to calculate the second-order wave force accurately along with the first-order loads to obtain the realistic combined effect of low-frequency wave loading on the overall system dynamics, which is underestimated without considering the second-order terms.

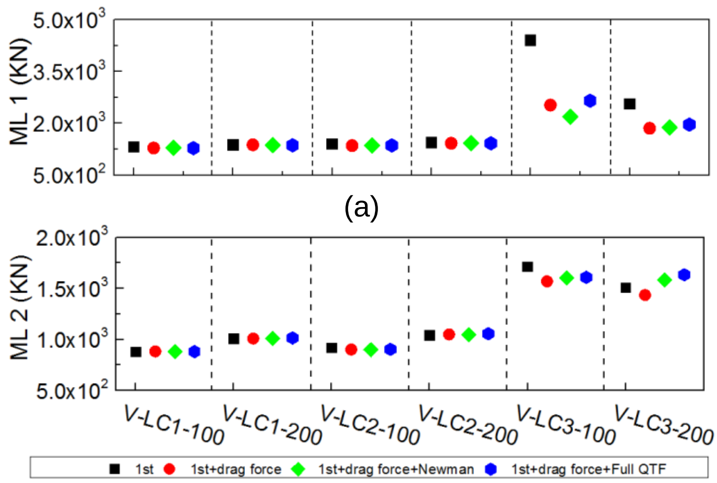

(b)

Figure 11. Maximum values of ML 1 and 2 for the V-shaped Semi. (a) ML 1; (b) ML 2.

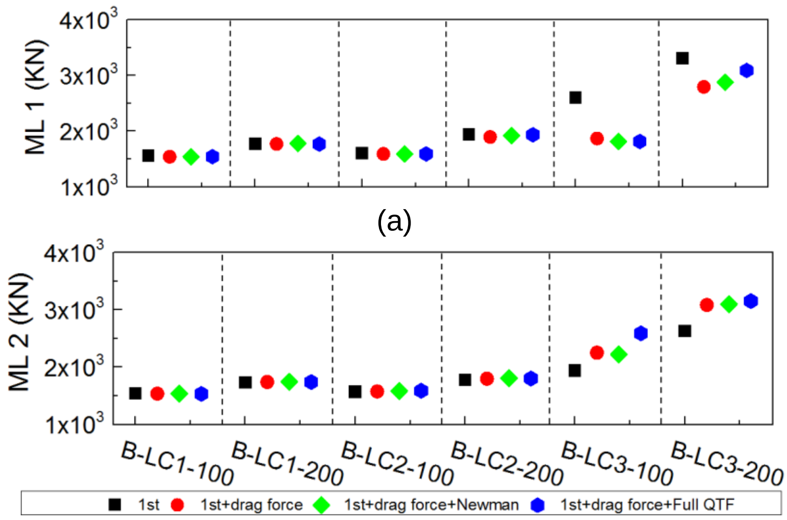

(a)

(b)

Figure 12. Maximum values of ML 1 and 2 for the Braceless Semi. (a) ML 1; (b) ML 2.

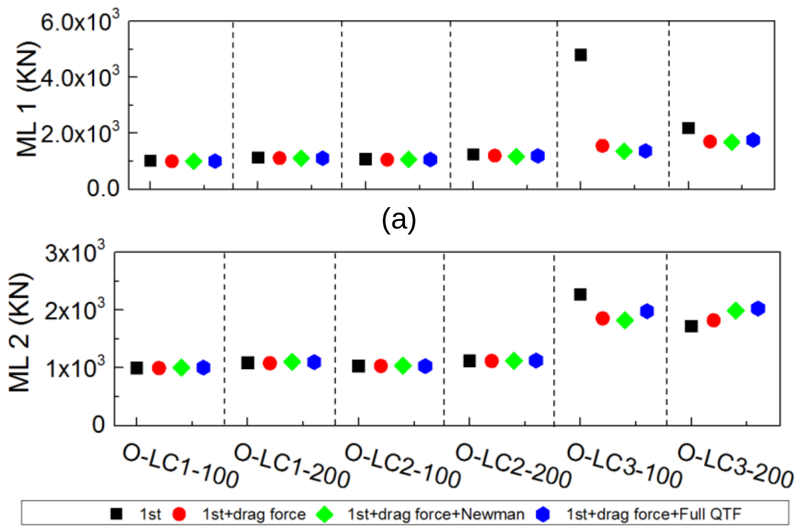

(a)

(b)

Figure 13. Maximum values of ML 1 and 2 for the OC4-DeepCwind Semi.(a) ML 1; (b) ML 2.

4.1.2 Mooring tension response

The maximum mooring line tensions for ML 1 and ML 2 are shown in Figure 11 to Figure 13. The standard deviation (STD) values of the mooring tension for the three semisubmersible FOWTs under the LC 1 and LC 3 conditions are shown in Table 9 and Table 10. Notably, there is a constant offset in the negative surge direction before reaching the static equilibrium for the V-shaped semisubmersible FOWT, while the Braceless and OC4-DeepCwind semisubmersible FOWTs do not have such an offset. Therefore, the pretension of ML 1 is larger than those of the other two mooring lines for the V-shaped semisubmersible FOWT.

The maximum values of the mooring line tension in extreme sea conditions, where the significant wave height is large, are relatively larger than those in moderate sea conditions for all semisubmersible FOWTs. The mooring line tension performance of the OC4-DeepCwind and V-shaped semisubmersible FOWT is similar at the two water depths, while the mooring line tension is larger at a water depth of 200 m than at a water depth of 100 m for the Braceless semisubmersible FOWT, as shown in Figure 11 to 13. Despite the small orders of magnitude for the drag force, it could reduce the motion response and then affect the mooring tension responses. As seen in the first-order solution, the maximum values and STD values of the mooring line tension are larger when ignoring the Morison drag force effect on the platform. Therefore, the drag term of the column should be thoroughly considered to better capture the actual mooring response for the three semisubmersible FOWT.

Table 9. STD values of the mooring tension responses for the three semisubmersible FOWTs under LC 1.

Tension	Method	V-100-LC1	V-200-LC1	B-100-LC1	B-200-LC1	O-100-LC1	O-200-LC1
ML 1	1st	***32.20***	22.94	***18.04***	24.96	***16.74***	24.58
	1st+drag force	***28.48***	22.27	***13.01***	25.41	***11.73***	21.58
	1st+drag force+Newman	29.02	22.54	13.92	25.53	15.04	23.24
	1st+drag force +Full QTF	29.32	22.55	14.74	26.33	15.42	23.89
ML 2	1st	20.62	17.66	12.38	18.68	8.74	12.33
	1st+drag force	20.06	17.55	10.68	18.81	6.41	10.88
	1st+drag force+Newman	20.46	17.96	11.04	19.08	8.24	12.34
	1st+drag force +Full QTF	20.46	17.96	11.29	19.31	8.42	12.65

Table 10. STD values of the mooring tension responses for the three semisubmersible FOWTs under LC 3.

Tension	Method	V-100-LC3	V-200-LC3	B-100-LC3	B-200-LC3	O-100-LC3	O-200-LC3
ML 1	1st	***332.78***	***185.75***	***201.71***	***329.27***	***338.24***	***239.72***
	1st+drag force	***207.95***	***156.07***	***141.55***	***287.68***	***124.49***	***175.16***
	1st+drag force+Newman	***186.64***	***150.84***	***144.28***	***287.45***	***98.54***	***153.34***
	1st+drag force +Full QTF	***202.04***	***163.30***	***150.87***	***296.16***	***103.52***	***169.42***
ML 2	1st	133.28	104.36	94.44	166.82	180.90	123.13
	1st+drag force	116.92	103.21	104.71	189.44	119.67	123.76
	1st+drag force+Newman	122.60	113.69	128.69	204.77	132.13	149.69
	1st+drag force +Full QTF	124.80	118.79	142.00	221.32	139.03	157.04

The second-order wave force could lead to large responses at resonance. Moreover, the second-order wave force did increase the maximum values and standard deviation values. As shown in Figures 10 to 12 and Tables 9 to 10, the maximum value, as well as the STD values of mooring force in a water depth of 100 m, is larger when using the full QTF method. Therefore, the effect of second-order wave force on the mooring line tension should be thoroughly considered when designing semisubmersible FOWT and mooring systems for moderate water depths.

From Tables 7, 8, 9 and 10, the STD results show that there is a good correlation between the mooring tension and surge motion. Comparing the STD values for forces of ML 1 to those for ML 2, 3 force reveals that ML 1 tension changed more dramatically than ML 2 and 3 tension for all semisubmersible FOWTs, which means that ML 1 is more sensitive to external loads. These results show that ML 1 is more susceptible to fatigue damage than other mooring lines and then causes the failure of the supporting platforms. For the mooring system design of semisubmersible FOWTs, especially for triangular platforms, the main mooring line should be strengthened to maintain the safety of the supporting structures.

4.2 Spectral analysis

This section presents the frequency-domain analysis results of the three semisubmersible FOWT with a 0-degree incoming wave direction under three load cases at two water depths. Four load models are listed together for comparison. The motion and mooring tension responses with and without drag force on the column are compared. For the second-order solution, the difference frequency wave loads using two methods (Newman's approximation and the full QTF method) are obtained to investigate the second-order wave force effect on the motion and mooring tension responses of semisubmersible FOWTs.

4.2.1 Natural frequencies of the three FOWTs

The natural frequency of the surge, heave and pitch motion for the three FOWTs are calculated by performing numerical decay tests in AQWA. Time series of free-decay tests on surge, heave and pitch motions can be obtained from AQWA output results. Then the natural frequency of the three FOWTs can be calculated based on the Fast Fourier Transform (FFT) method (Cooley *et al*., 1969), as shown in Table 11.

Table 11. Natural frequency for the three semisubmersible FOWTs

Modes	V-shaped Semi	Braceless Semi	OC4-DeepCwind Semi
Surge (100/200 m) rad/s	0.086/0.067	0.080/0.083	0.058/0.050
Heave (100/200 m) rad/s	0.241/0.238	0.249/0.241	0.376/0.364
Pitch (100/200 m) rad/s	0.327/0.326	0.201/0.201	0.251/0.251

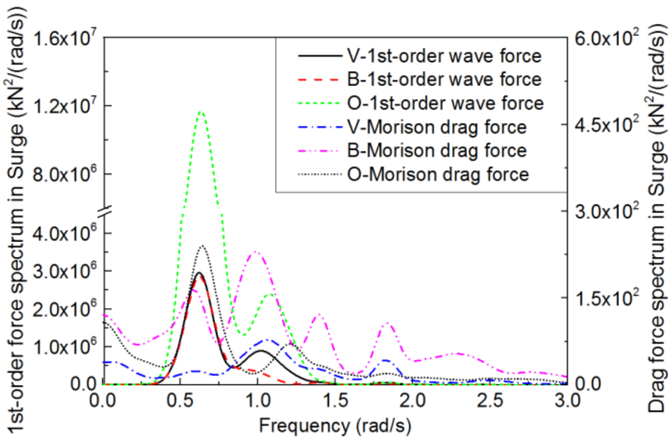

Figure 14. Comparison between drag force and first-order wave force (LC 1) in frequency domain of surge motion for the three semisubmersible FOWTs.

4.2.2 Hydrodynamic load spectrum

A comparison between the drag force and first-order wave force of the three semisubmersible FOWTs in the LC 1 condition at a 100-m water depth is shown in Figure 14. As shown in Figure 14, compared to the first-order wave force, the drag force is very small. Even though the drag force is small, its resonant effect can be significant. A comparison between the first-order wave force and drag force in the frequency-domain shows that the drag force is more broad-banded than the first-order force, which could cause large resonance in the low-frequency region especially for surge mode.

Figure 15 shows a comparison of the second-order wave force among the three semisubmersible FOWTs under moderate sea condition (LC 1) by using Newman's approximation and the full QTF method. The results show that the power spectral density is mainly concentrated in the difference-frequency region when using Newman's approximation, while two peaks appear in the difference-frequency and sum-frequency region when using the full QTF method. Although the natural frequencies of the structure are designed to be outside the first-order wave energy spectrum, the second-order loads may excite these frequencies. The difference-frequency is close to the natural frequency of the structures for semisubmersible FOWTs. As shown in Figure 15(b), second-order responses in the difference-frequency region are higher when using the full QTF method than when using to Newman's approximation method of the V-shaped semisubmersible and Braceless semisubmersible FOWT, while the responses obtained using the two methods are similar for the OC4-DeepCwind semisubmersible FOWT. This set of data indicates that the second-order force calculated by the full QTF method can greatly excite heave motion response for the V-shaped semisubmersible and Braceless semisubmersible FOWTs. Figure 15(c) shows that, in the difference-frequency region, the second-order force responses computed using the full QTF method were higher than the responses computed using Newman's approximation method for the OC4-DeepCwind semisubmersible FOWT. The result indicates that the pitch motion of OC4-DeepCwind semisubmersible is more sensitive than that of the other two platforms when considering the second-order wave force.

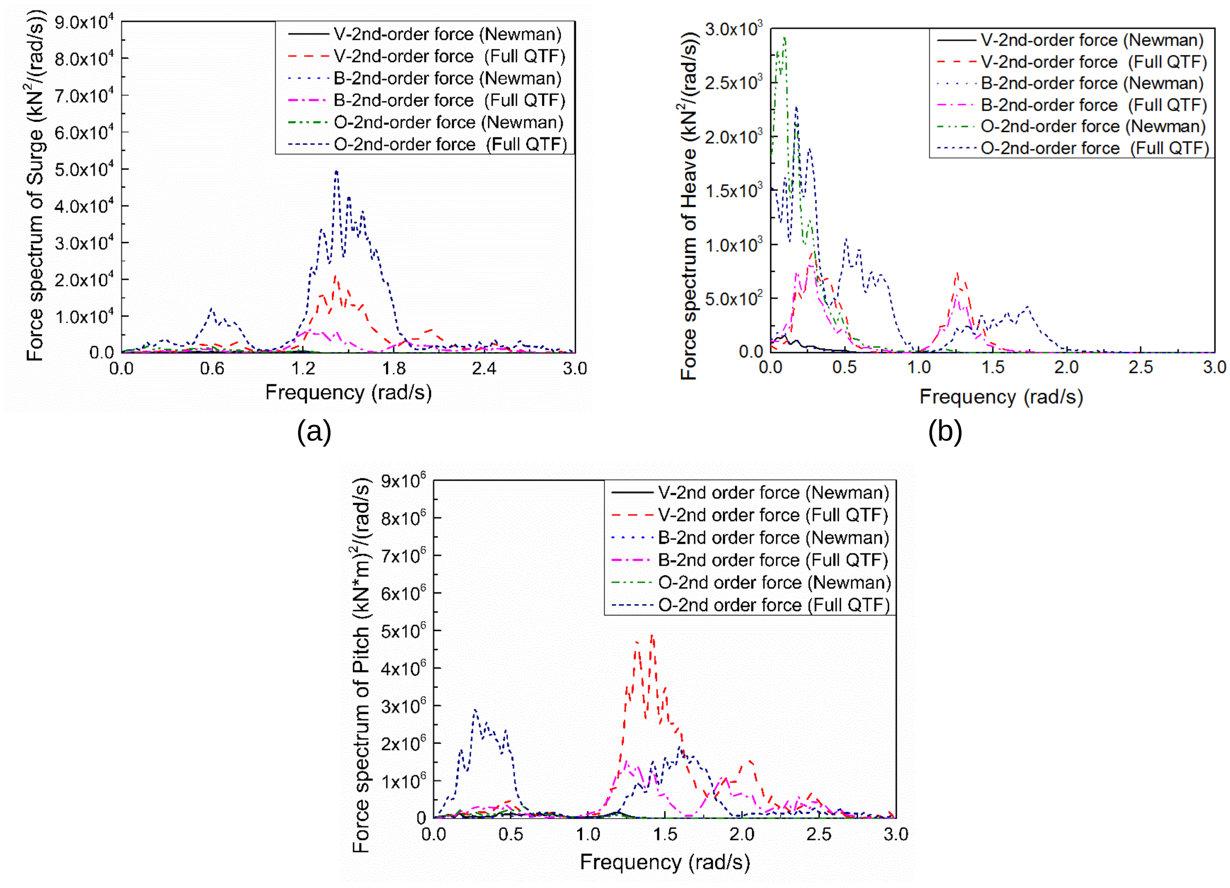

(c)

Figure 15. Comparison of the second-order wave force in the frequency-domain using different methods for the three semisubmersible FOWTs. (a) Surge; (b) Heave; (c) Pitch.

4.2.3 Motion spectrum

For moderate sea conditions, there is a great similarity regarding the power spectra density (PSD); therefore, only the spectrum results in the LC 1 condition are listed. Figure 16 to Figure 18 show the motion spectrum of the three semisubmersible FOWTs in the LC 1 at two water depths.

(1) For surge motion, the spectra of the motion responses consist of two parts: the low-frequency part is related to the surge natural frequency while the higher frequency part is

dominated by the frequency from 0.4 to 0.8 rad/s which is related to the wave peak frequency. For the first-order solution, the surge resonance peak decreases significantly due to the drag force on each column compared to the first line as shown in Figure 16. This is similar to what is observed for the other platforms (Figure 16(b) and Figure 16(c)).

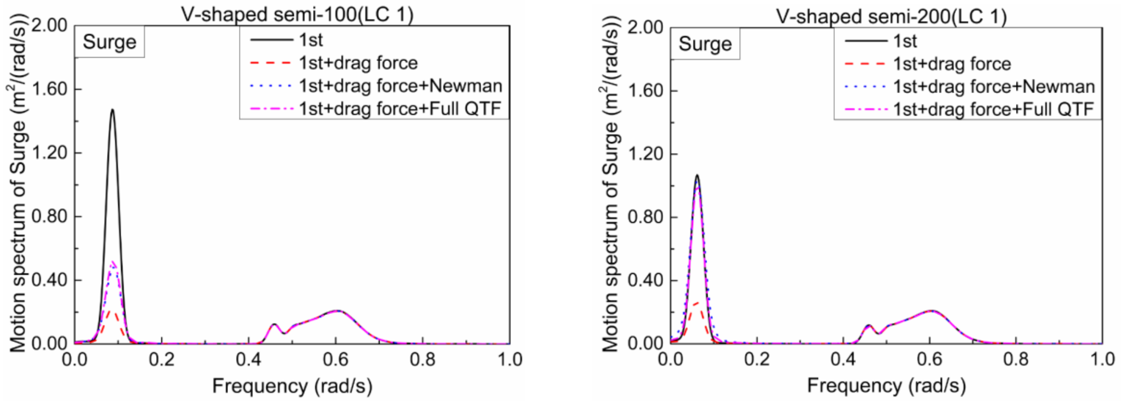

(a)

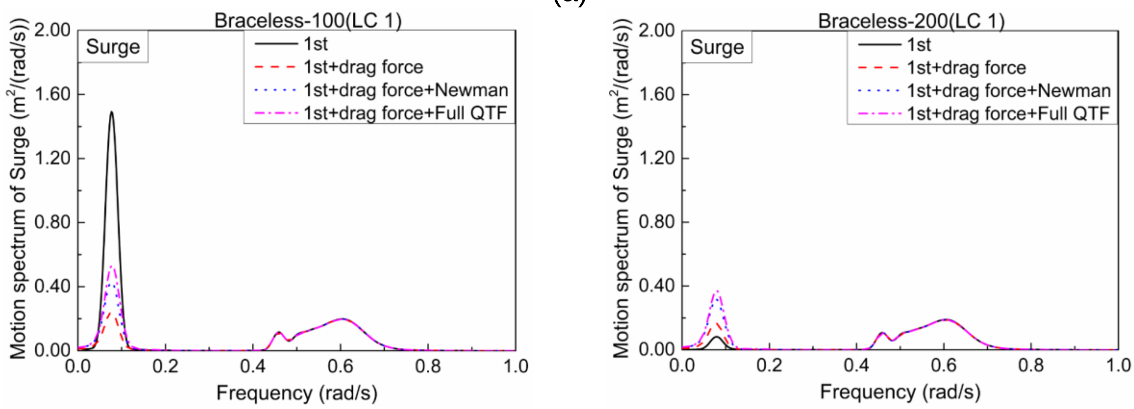

(b)

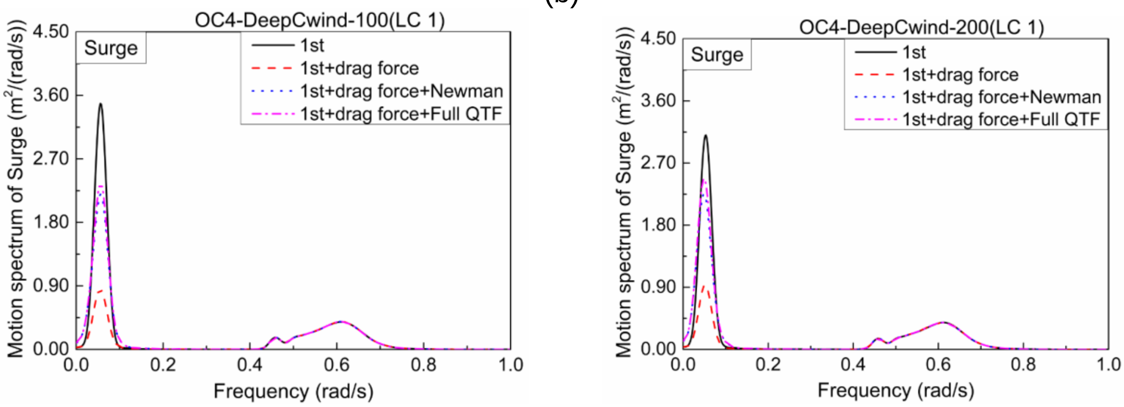

(c)

Figure 16. Floater surge motion spectrum of the semisubmersible FOWTs in LC 1 condition. (a) V-shaped Semi; (b) Braceless Semi; (c) OC4-DeepCwind Semi.

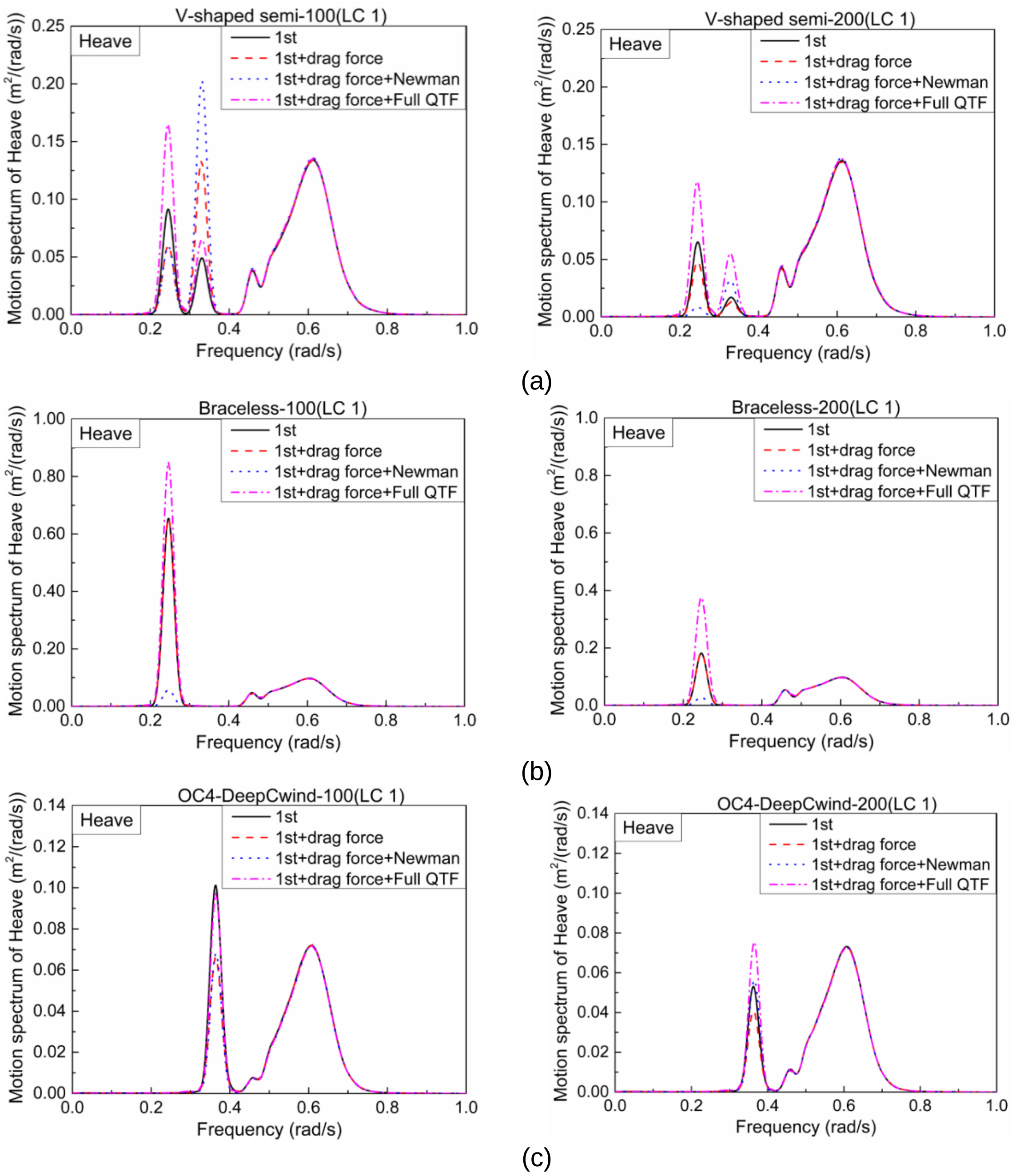

Figure 17. Floater heave motion spectrum of semisubmersible FOWTs in LC 1 condition. (a) V-shaped Semi; (b) Braceless Semi; (c) OC4-DeepCwind Semi.

(2) For heave motion, the wave frequency response still dominates in the same range, which is approximately 0.4 rad/s to 0.8 rad/s. A large response also occurs at the heave natural frequency of each semisubmersible FOWT (Figure 17(b), Figure 17(c)). In contrast to the other two semisubmersible platforms, the V-shaped semisubmersible FOWT exhibited two peaks (Figure 17(a)), which are close to the pitch and heave natural frequencies, showing the coupling between pitch and heave motions. It is also observed that the wave frequency response is larger in the 100-m case than in the 200-m case. For the first-order solution, the

difference in the heave motion response among the three semisubmersible floating platforms is small with and without the Morison drag force on the column. Comparing the difference-frequency response obtained by using Newman's approximation and the full QTF method clearly reveals that the heave motion response is underestimated for Newman's approximation solution in the V-shaped semisubmersible FOWT and Braceless semisubmersible FOWT (Figure 17(a) and Figure 17(b)). By contrast, for the OC4-DeepCwind semisubmersible FOWT, the difference in the heave motion response between Newman's approximation and the full QTF method is smaller than that for the other two semisubmersible floating platforms.

(3) For pitch motion, different from the other modes, the spectra of the motion responses are mainly dominated by the response at the pitch natural frequency. For the V-shaped semisubmersible FOWT (Figure 18(a)), there are two peaks in the low-frequency region, which are at the pitch and heave natural frequencies, showing the coupling effect of these two modes. For the Braceless and OC4-DeepCwind semisubmersible FOWTs, the spectra of the motion responses consist of two parts: the low-frequency part is related to the pitch natural frequency while the higher frequency part is dominated by the frequency of 0.4 to 0.8 rad/s which is related to the wave peak frequency. For the second-order solution, the difference-frequency wave force can greatly excite the resonance of the pitch mode response when using the full QTF method. As seen in the plots, the peak value at pitch natural frequency is higher in full-QTF solution, which causes large pitch responses for the three semisubmersible FOWTs as shown in Figures 8(c), 9(c) and 10(c).

Comparing the values with and without the drag force reveals that dynamic response of surge motion can be greatly decreased by adding the Morison drag force on the column. Therefore, it is vitally significant to consider the drag term when designing and performing the computation of semisubmersible FOWTs. Newman's approximation method is suitable for surge resonant motion response, while it doesn't apply to the heave or pitch resonant responses. It can be seen from Figures 16 and 17 that the heave and pitch resonant response in the low-frequency region is underestimated. Therefore, the full QTF method should be used for modelling the difference-frequency wave force to better simulate the low-frequency motion.

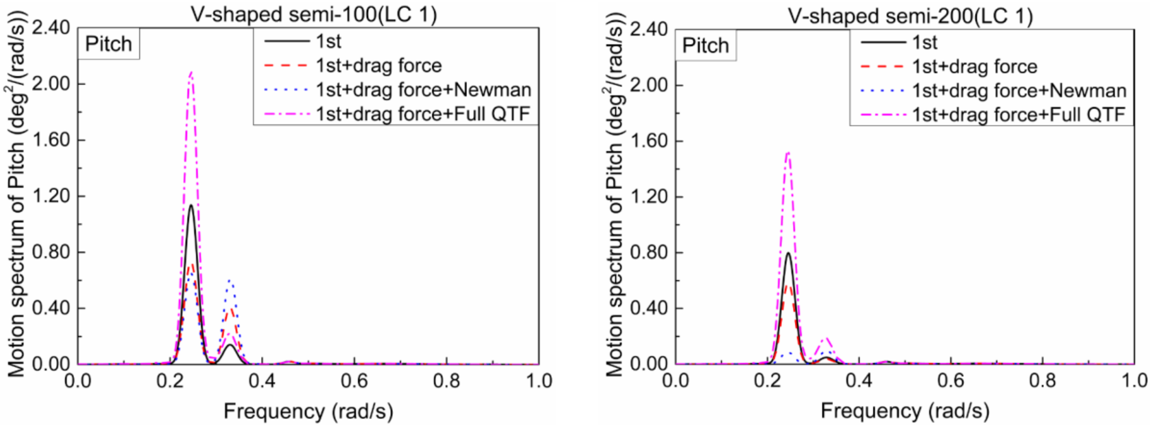

(a)

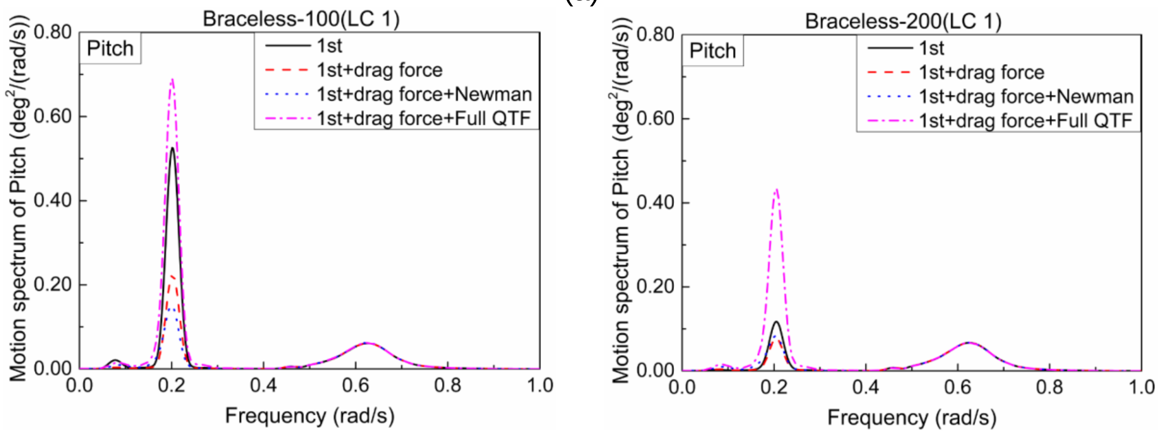

(b)

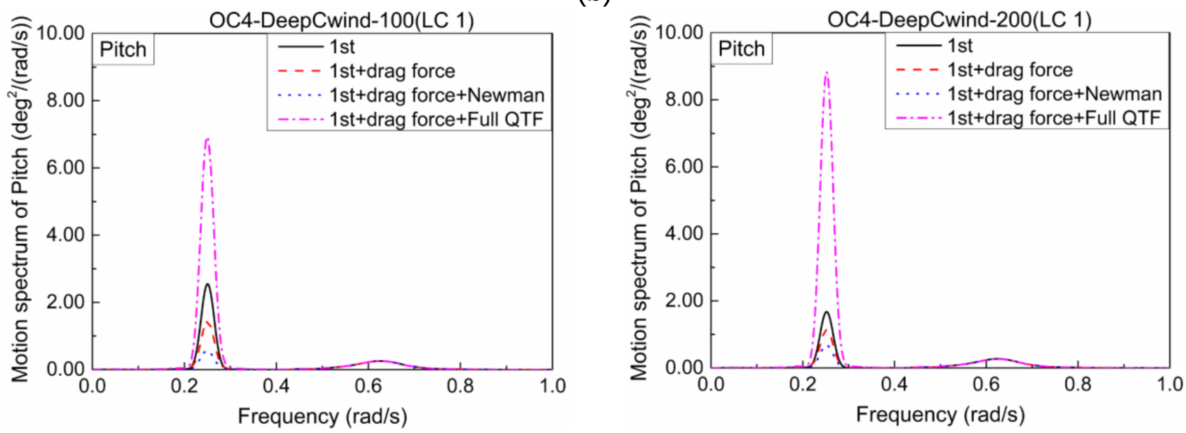

(c)

Figure 18. Floater motion spectrum of semisubmersible FOWTs in the LC 1 condition.

(a) V-shaped Semi; (b) Braceless Semi; (c) OC4-DeepCwind Semi.

4.2.4 Mooring tension spectrum

The mooring line responses in the frequency domain in the head for sea under the LC 1 condition of the three semisubmersible FOWTs are shown in Figure 19 to 21. Due to the symmetry of the mooring line configuration of the three platforms, only the mooring line responses of ML 1 and ML 2 are displayed in this paper.

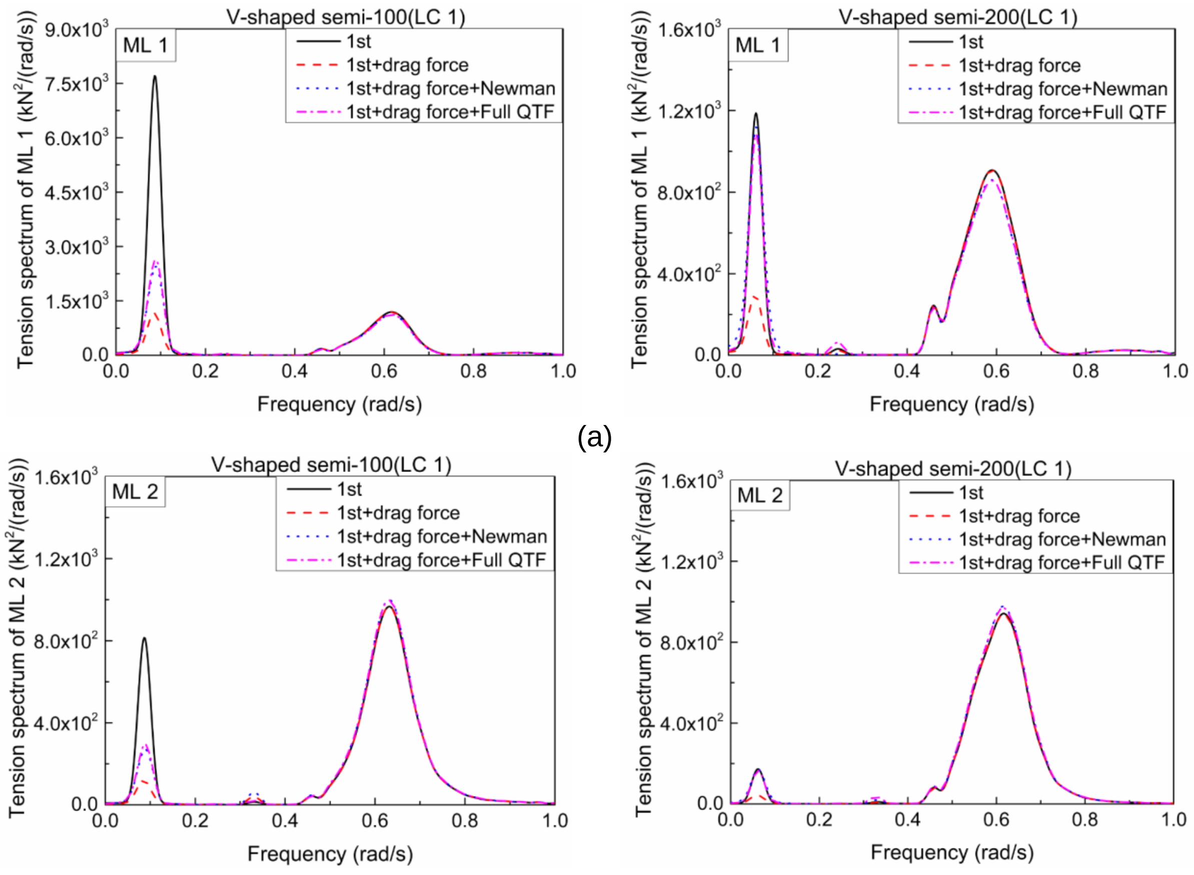

Figure 19. Mooring tension spectrum of the V-shaped Semi in LC 1 condition. (a) ML 1; (b) ML 2.

For the V-shaped semisubmersible FOWT, the most significant contribution to the ML 1 tension comes from wave frequency range from 0.4 rad/s to 0.8 rad/s, while for ML 2 and 3, the most significant contribution comes from the low-frequency region (surge motion response). The contribution from the low-frequency response increases with decreasing water depth. A small peak is observed at approximately 0.25 rad/s (pitch natural frequency) showing the coupling effect between surge and pitch modes. The first-order solution results show that the effect of drag force on the column becomes more significant as the water depth decreased. It can also be seen that second-order surge resonant responses (Figure 19) seem similar when using the two methods to perform the calculations of the difference-frequency wave force at both water depths.

For the Braceless semisubmersible FOWT, the mooring line tension responses consist of two parts: the wave frequency range from 0.4 rad/s to 0.8 rad/s and the low-frequency region including the surge, pitch and heave mode response. Similar to the V-shaped semisubmersible FOWT, the contribution from the low-frequency response increases while the high-frequency response (wave frequency) decreases. For the second-order solution, the surge resonant responses are slightly higher when using the full QTF method than when using the Newman's approximation to perform the difference-frequency wave force calculation.

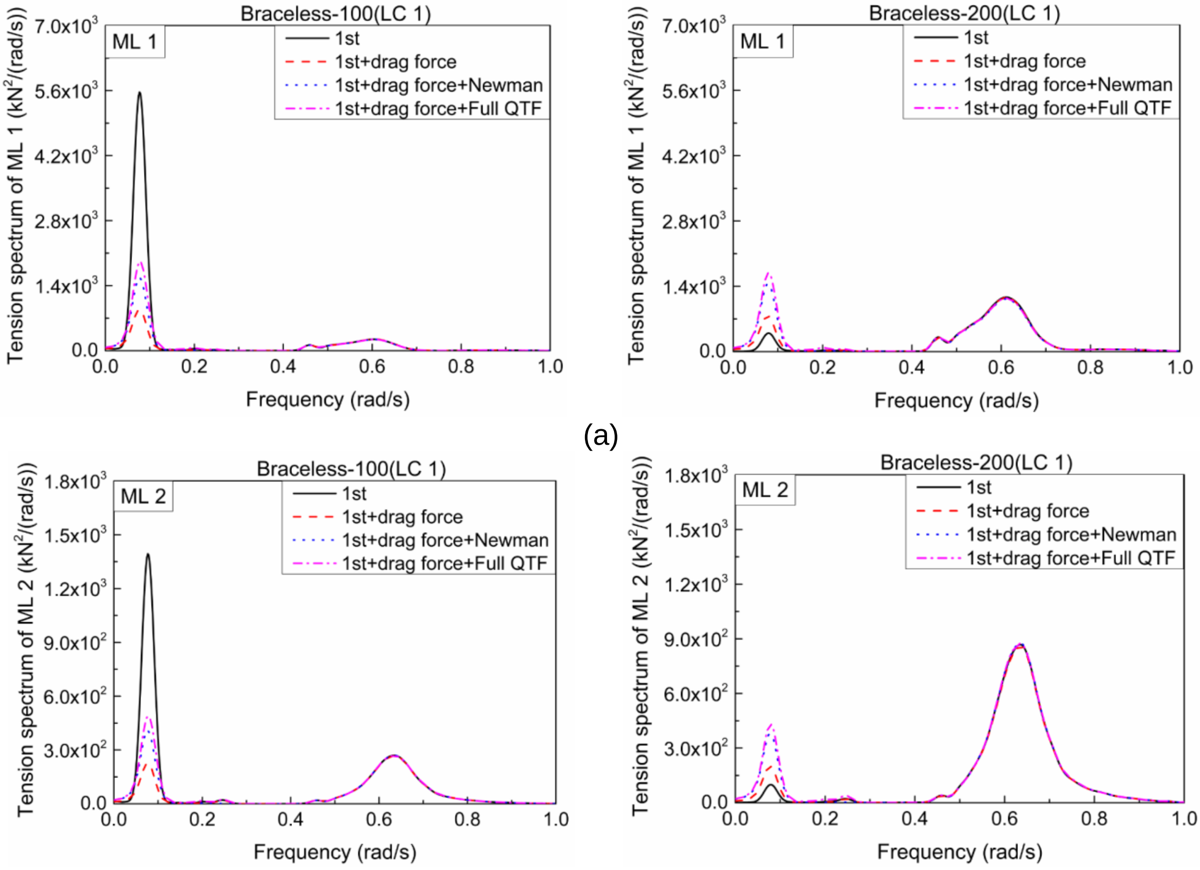

Figure 20. Mooring tension spectrum of the Braceless Semi in LC 1 condition. (a) ML 1; (b) ML 2.

For the OC4-DeepCwind semisubmersible FOWT, in contrast to the other two platforms, the most significant contribution to the mooring line tension comes from the low-frequency region. The coupling effect between structural modes, including the surge and pitch modes is shown in Figure 21. Compared to the other two platforms, the OC4-DeepCwind semisubmersible FOW show similar performance in the dynamic response of mooring line tension in the frequency-domain at the two water depth. Similar to the Braceless semisubmersible FOWT, surge resonant responses are slightly higher when using the full QTF method than when using Newman's approximation method to calculate the difference-frequency wave force.

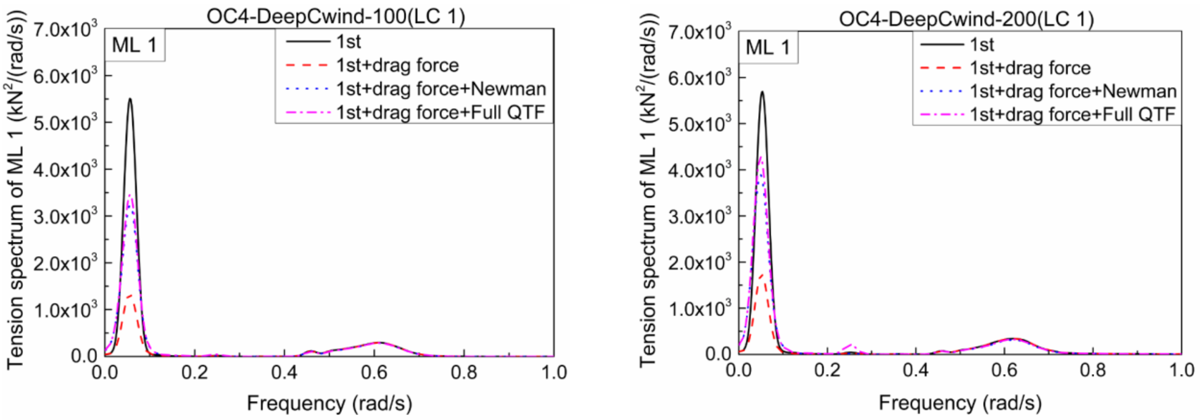

(a)

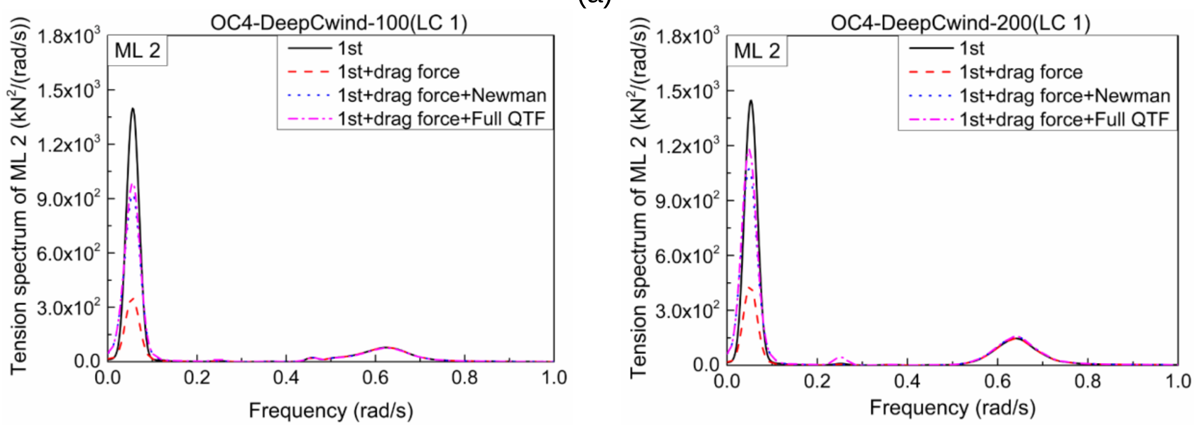

(b)

Figure 21. Mooring tension spectrum of the OC4-DeepCwind Semi in the LC 1 condition. (a) ML 1; (b) ML 2.

5. Conclusions

In this paper, a comparative study of hydrodynamic performance among the V-shaped semisubmersible, Braceless semisubmersible and OC4-DeepCwind semisubmersible FOWT sunder different water depths is performed considering second-order hydrodynamic loads. Spectra and the time-domain response of platform motions and mooring tension are presented. The discussion has been made and useful conclusions can be summarized in the following aspects:

For the dynamic motion response, the result shows that the difference-frequency wave force can excite the responses at the natural frequency of all the semisubmersible FOWTs, especially for the pitch motion. Also, the results indicate that the pitch motion of OC4-DeepCwind semisubmersible FOWT is more sensitive than that of the other two semisubmersible FOWTs when considering the second-order wave loads. The STD value of the motion responses show that, compared with the Newman's approximation method, the STD values of pitch motion (LC 3) under water depth of 200 m for the semisubmersible FOWTs, including the V-shaped semisubmersible FOWT, Braceless semisubmersible FOWT and OC4-DeepCwind semisubmersible FOWT increased by 68.0%, 32.5% and 183.4% respectively using the full-QTF method. Moreover, the first-order results show that the surge motion response decreases when considering the Morison drag term on the column. Therefore, the full QTF method is recommended to calculate the difference-frequency wave force since the Newman's approximation could underestimate the motion response. Also, the Morison drag term should be used for better simulating the actual motion responses.

The dynamic mooring tension response is mainly dominated by the response close to the surge natural frequency and wave frequency range. Compared to mooring tension of ML 2 and ML 3, the STD values of the mooring tension show that ML 1 is more sensitive. For the first-order solution, the mooring tension is overestimated when ignoring the Morison drag term on the column. As it is can be seen in Table 10, under the extreme sea condition, the ML 1 tension of the V-shaped semisubmersible, Braceless semisubmersible and OC4-DeepCwind semisubmersible FOWT is decreased by 16.0%, 12.9% and 26.9%, respectively, in the water depth of 200 m. For the second-order solution, compared to Newman's approximation solution, dynamic mooring tension response is more severe in the full QTF solution.

For the dynamic response under different water depth, the results show that the motion and mooring tension response is larger in the moderate water depth, which could cause fatigue damage in long term and then threaten the safety of FOWTs. And the results also show that the contribution of second-order wave forces increasing when the water depth decreases, especially for pitch motion. The comparative results of the motion performance for three semisubmersible FOWTs in different water depth showing that the Braceless semisubmersible FOWT is more sensitive to the change of water depth. As shown in Figure 4, the heave motion response of OC4-DeepCwind semisubmersible is larger than that of the other two semisubmersible FOWT for the extreme sea condition, for the reason that the natural frequency of heave mode is close to the normal wave frequency range, which causes large resonance in the OC4-DeepCwind semisubmersible FOWT. Therefore, the heave natural frequency of the OC4-DeepCwind semisubmersible FOWT should be thoroughly considered.

ACKNOWLEDGEMENT

This research was funded by the National Natural Science Foundation of China (Grant No. 51709039, 51709040). This work is also partially supported by the international collaboration and exchange program from the NSFC-RCUK/EPSRC with grant No. 51761135011. This work is also partially supported by LiaoNing Revitalization Talents Program (XLYC1807208) and the Fundamental Research Funds for the Central University (DUT19GJ209).

References

DeCastro, M., Salvador, S., Gómez-Gesteira, M., Costoya, X., Carvalho, D., Sanz-Larruga, F. J., and Gimeno, L. (2019). Europe, China and the United States: Three different approaches to the development of offshore wind energy. Renewable and Sustainable Energy Reviews, 109, 55-70.

Shi, W., Park, H. C., Chung, C. W., Shin, H. K., Kim, S. H., Lee, S. S., and Kim, C. W. (2015). Soil-structure interaction on the response of jacket-type offshore wind turbine. *International Journal of Precision Engineering and Manufacturing-Green Technology*, *2*(2), 139-148.

Shi, W., Tan, X., Gao, Z., and Moan, T. (2016). Numerical study of ice-induced loads and responses of a monopile-type offshore wind turbine in parked and operating conditions. *Cold Regions Sci Tech*, *123*, 121-139.

Mo, R., Kang, H., Li, M., and Zhao, X. (2017). Seismic fragility analysis of monopile offshore wind turbines under different operational conditions. *Energies*, *10*(7), 1037.

Chian, C. Y., Zhao, Y. Q., Lin, T. Y., Nelson, B., and Huang, H. H. (2018). Comparative study of time-domain fatigue assessments for an offshore wind turbine jacket substructure by using conventional grid-based and Monte Carlo sampling methods. *Energies*, *11*(11), 3112.

Hong, L., and Möller, B. (2011). Offshore wind energy potential in China: under technical, spatial and economic constraints. *Energy*, *36*(7), 4482-4491.

Driscoll, F., Jonkman, J., Robertson, A., Sirnivas, S., Skaare, B., and Nielsen, F. G. (2016). Validation of a FAST model of the statoil-hywind demo floating wind turbine. *Energy Procedia*, *94*, 3-19.

Maciel, J. G. (2010). The WindFloat Project. EDP: Lisbon, Portugal.

Boccard, N. (2014). The cost of nuclear electricity: France after Fukushima. *Energy Policy*, *66*, 450-461.

Skaare, B. (2017). Development of the hywind concept. In *ASME 2017 36th International Conference on Ocean, Offshore and Arctic Engineering* . American Society of Mechanical Engineers.

Roddier, D., Cermelli, C., Aubault, A., and Weinstein, A. (2010). WindFloat: A floating foundation for offshore wind turbines. *Journal of renewable and sustainable energy*, 2(3), 033104.

Huijs, F., de Bruijn, R., and Savenije, F. (2014). Concept design verification of a semi-submersible floating wind turbine using coupled simulations. *Energy Procedia*, *53*, 2-12.

Lefranc, M., and Torud, A. (2011). Three wind turbines on one floating unit, feasibility, design and cost. In *Offshore Technology Conference*. Offshore Technology Conference.

Le Boulluec, M., Ohana, J., Martin, A., and Houmard, A. (2013,). Tank testing of a new concept of floating offshore wind turbine. In *ASME 2013 32nd international conference on Ocean, offshore and arctic engineering*. American Society of Mechanical Engineers Digital Collection.

Luan, C., Gao, Z., and Moan, T. (2016). Design and analysis of a braceless steel 5-mw semi-submersible wind turbine. In *ASME 2016 35th International Conference on Ocean, Offshore and Arctic Engineering*. American Society of Mechanical Engineers Digital Collection.

Antonutti, R., Peyrard, C., Johanning, L., Incecik, A. and Ingram, D.(2016). The Effects of Wind-Induced Inclination On the Dynamics of Semi-Submersible Floating Wind Turbines in the Time Domain. *Renewable Energy, 88*, 83-94.

Jiang, Y., Hu, G., Jin, G., Sun, Z., Li, J. and Zong, Z.(2018). Hydrodynamic Performance of a Novel Floating Foundation for Offshore Wind Turbine. *The 28th International Ocean and Polar Engineering Conference*.

Shi, W., Zhang L., Ning, D., Jiang Z., Michailies, C., and Karimirad, M. (2019). A comparative study on dynamic response of different semi floating offshore wind turbines. In *ASME 2019 38th International Conference on Ocean, Offshore and Arctic Engineering.* American Society of Mechanical Engineers.

Zhao, Z., Li, X., Wang, W., Shi, W., 2019. Analysis of Dynamic Characteristics of an Ultra-Large Semi-Submersible Floating Wind Turbine. *Journal of Marine Science and Engineering*. *7(6)*, 169.

Roald, L., Jonkman, J., Robertson, A., Chokani, N., 2013. The Effect of Second-Order Hydrodynamics On Floating Offshore Wind Turbines. *Energy Procedia, 35*, 253-264.

Coulling, A.J., Goupee, A.J., Robertson, A.N. and Jonkman, J.M.(2013). Importance of Second-Order Difference-Frequency Wave-Diffraction Forces in the Validation of a Fast Semi-Submersible Floating Wind Turbine Model. *ASME 2013 32nd International Conference on Ocean, Offshore and Arctic Engineering*. American Society of Mechanical Engineers.

Li, J., Jiang, Y., Tang, Y., Qu, X., and Zhai, J. (2017). Effects of Second-Order Difference-Frequency Wave Forces on Floating Wind Turbine under Survival Condition. *Transactions of Tianjin University*, *23*(2), 130-137.

Xu, K., Gao, Z., and Moan, T. (2018). Effect of hydrodynamic load modelling on the response of floating wind turbines and its mooring system in small water depths. In *Journal of Physics: Conference Series* (Vol. 1104, No. 1, p. 012006). IOP Publishing.

Gueydon, S., Duarte, T., and Jonkman, J. (2014). Comparison of second-order loads on a semisubmersible floating wind turbine. In *ASME 2014 33rd International Conference on Ocean, Offshore and Arctic Engineering*. American Society of Mechanical Engineers Digital Collection.

Bayati, I., Jonkman, J., Robertson, A., and Platt, A. (2014). The effects of second-order hydrodynamics on a semisubmersible floating offshore wind turbine. In *Journal of Physics: Conference Series* (Vol. 524, No. 1, p. 012094). IOP Publishing.

ANSYS Inc. ANSYS AQWA, 2017, Line, Librium, NAUT and Tether Manuals; Pittsburgh, CO, USA, 2017.

Faltinsen, O. (1993). *Sea loads on ships and offshore structures* (Vol. 1). Cambridge university press.

Teng, B. Wave action on maritime structures, 3rd ed; Ocean press, Beijing, China, 2015.

Newman, J. T. (1967). The drift force and moment on ships in waves. *Journal of ship research*, *11*(01), 51-60.

Fonseca, N., Pessoa,J., and Guedes Soares,C. (2008). Calculation of second order drift forces on a FLNG accounting for difference frequency components. In *ASME 2008 27th International Conference on Ocean, Offshore and Arctic Engineering*. American Society of Mechanical Engineers Digital Collection.

Pessoa J, Fonseca N, Guedes Soares C. (2010). Experimental and Numerical Study of the

Depth Effect on the First-order and Slowly Varying Motions of a Floating Body in Bichromatic Waves. In *ASME 2010 29th International Conference on Ocean, Offshore and Arctic Engineering*. American Society of Mechanical Engineers Digital Collection.

Pinkster, J. A. (1975). Low-frequency phenomena associated with vessels moored at sea. *Society of Petroleum Engineers Journal*, *15*(06), 487-494.

Hall, M., and Goupee, A. (2015). Validation of a lumped-mass mooring line model with DeepCwind semisubmersible model test data. *Ocean Engineering*, *104*, 590-603.

Jonkman, J., Butterfield, S., Musial, W., and Scott, G. (2009). *Definition of a 5-MW reference wind turbine for offshore system development.* National Renewable Energy Laboratory.

Forward, F. (2014). Fukushima Floating Offshore Wind Farm Demonstration Project. Japan: Fukushima Offshore Wind Consortium.

Karimirad, M., and Michailides, C. (2015). V-shaped semisubmersible offshore wind turbine: An alternative concept for offshore wind technology. *Renewable Energy*, *83*, 126-143.

Karimirad, M., and Michailides, C. (2016). V-shaped semisubmersible offshore wind turbine subjected to misaligned wave and wind. *Journal of Renewable and Sustainable Energy*, *8*(2), 023305.

Borisade, F. (2016). Qualification of Innovative Floating Substructures for 10 MW Wind Turbines and Water Depths Greater than 50 m–D 7.4: State-of-the-Art FOWT Design Practice and Guidelines. *European Union*.

Luan, C. (2018). Design and analysis for a steel Braceless semi-submersible hull for supporting a 5-MW horizontal axis wind turbine, PhD theses, Norwegian University of Science and Technology, Trondheim, Norway, 2018.

Robertson, A., Jonkman, J., Masciola, M., Song, H., Goupee, A., Coulling, A., and Luan, C. (2014) Definition of the semisubmersible floating system for phase II of OC4. National Renewable Energy Laboratory.

Jeon, S. H. , Cho, Y. U. , Seo, M. W. , Cho, J. R. , and Jeong, W. B. (2013). Dynamic response of floating substructure of spar-type offshore wind turbine with catenary mooring cables. *Ocean Engineering, 72*, 356-364.

Li, L., Gao, Z., and Moan, T. (2015). Joint distribution of environmental condition at five european offshore sites for design of combined wind and wave energy devices. *Journal of Offshore Mechanics and Arctic Engineering*, *137*(3), 031901.

Wind, G. L. (2005). Guideline for the certification of offshore wind turbines. *Germanischer Lloyd Industrial Services GmbH.*

Cooley, J. W., Lewis, P. A., and Welch, P. D. (1969). The fast Fourier transform and its applications. *IEEE Transactions on Education*, *12*(1), 27-34.